THESIS FOR THE DEGREE OF LICENTIATE OF ENGINEERING

Probing the Effects of Conformation on the Photophysics of Conjugated Porphyrin Oligomers

MÉLINA GILBERT

Department of Chemical and Biological Engineering

CHALMERS UNIVERSITY OF TECHNOLOGY

Göteborg, Sweden 2013

Probing the Effects of Conformation on the Photophysics of Conjugated Porphyrin Oligomers

MÉLINA GILBERT

Ny serie nr 2013:3.

ISSN nr: 1652-943X

Department of Chemical and Biological Engineering

CHALMERS UNIVERSITY OF TECHNOLOGY

SE-412 96 Göteborg

Sweden

Telephone +46 (0) 31-772 1000

Cover picture: Top: Hypothetical structure of the fullerene and ferrocene appended porphyrin tetramer aggregate forming at low temperature. Bottom: (right) Structure of the fullerene appended porphyrin hexamer $\mathbf{P_6}C_{60}$ and (left) 3D streak camera image of the emission of twisted conformations of $\mathbf{P_6}C_{60}$.

Chalmers Reproservice

Göteborg, Sweden 2013

Probing the Effects of Conformation on the Photophysics of Conjugated Porphyrin Oligomers

MÉLINA GILBERT

Department of Chemical and Biological Engineering

CHALMERS UNIVERSITY OF TECHNOLOGY

Abstract

Controlling the conformational heterogeneity of molecular systems is fundamental to envisage future applications of these systems, such as in solar cells or molecular devices to name a few. The work presented in this Thesis investigates the effects of conformational flexibility on the photophysical properties of a series of conjugated porphyrin oligomers $\mathbf{P_n}$ (n = 1-4, 6, 8). First the influence of temperature on the conformational distribution displayed by these systems has been explored. At low temperature, these porphyrins spontaneously form highly-ordered planar aggregates resulting in characteristic changes in their spectral properties. The observed spectral changes could be explained by a planarization of the oligomers accompanying the aggregate formation. Further the influence of conformation on the electron transfer reactions in long fullerene-appended porphyrin oligomers $\mathbf{P_n}C_{60}$ (n = 4, 6) was studied thoroughly. The rate of charge separation could be tuned by selective excitation of different populations of conformations. Twisted conformations showed faster charge separation rates and higher efficiencies than planar conformations. The disparity in charge separation rates was ascribed to the differences in driving force for charge separation between twisted and planar conformations. The conformational distribution of $\mathbf{P_n}C_{60}$ systems could also be restrained and controlled by means of coordination to an octadentate ligand $\mathbf{T_8}$, thus providing simpler model systems to investigate the influence of conformation on the charge separation. The semi-circular complexes $\mathbf{P_n}C_{60}$-$\mathbf{T_8}$ showed significant differences in their spectral properties compared to their linear counterparts that were attributed to their planarity and higher rigidity. Charge separation was also investigated in these semi-circular complexes. These complexes displayed an extremely slow rate of charge separation and low efficiency of charge separation. The reason for this slow charge separation was the lack of driving force for charge separation to occur, as expected for more planar conformations.

Keywords: conjugated porphyrin oligomers, electron transfer, conformational analysis.

List of Publications

I. Kärnbratt, J.; Gilbert, M.; Sprafke, J. K.; Anderson, H. L.; Albinsson, B.
Self-Assembly of Linear Porphyrin Oligomers into Well-Defined Aggregates.
J. Phys. Chem. C **2012,** *116* (37), 19630-19635

II. Gilbert, M.; Anderson, H. L.; Albinsson, B.
Conformational Gating of Charge Separation in Porphyrin Oligomer-Fullerene Systems.
Manuscript

Contribution Report

Paper I: Performed some of the temperature-dependent absorption measurements, and helped in writing the paper.

Paper II: Performed all experiments and data analysis, and wrote the manuscript.

Contents

1. INTRODUCTION 1

2. THEORY 3

PHOTOPHYSICS 3

ELECTRON TRANSFER THEORY 6

THE DRIVING FORCE 7

THE REORGANIZATION ENERGY 8

THE ELECTRONIC COUPLING 9

3. PORPHYRIN MOLECULAR SYSTEMS INSPIRED BY NATURE 11

NATURAL PHOTOSYNTHESIS VERSUS ARTIFICIAL PHOTOSYNTHESIS 11

PORPHYRINS 13

THE DONOR-ACCEPTOR SYSTEMS STUDIED 14

4. SYNOPSIS 17

PAPER I: SELF-ASSEMBLY OF LINEAR PORPHYRIN OLIGOMERS INTO WELL-DEFINED AGGREGATES. 17

STEADY-STATE METHODS 17

SELF-ASSEMBLED PORPHYRIN OLIGOMERS 19

PAPER II: CONFORMATIONAL GATING OF CHARGE SEPARATION IN PORPHYRIN OLIGOMER-FULLERENE SYSTEMS 25

TIME-RESOLVED METHODS 25

INFLUENCE OF CONFORMATIONAL DYNAMICS ON ELECTRON TRANSFER IN PORPHYRIN OLIGOMER-FULLERENE SYSTEMS 29

5. SUMMARY AND FUTURE PERSPECTIVE **37**

6. ACKNOWLEDGEMENTS **39**

7. REFERENCES **41**

1. Introduction

Today one of the biggest challenges the world faces is the rising global consumption of energy. The International Energy Agency (IEA) projects this figure to increase from 140 x 10^3 TWh in 2007 to 195 x 10^3 TWh by 2030.[1] Currently about 80 % of the world's energy supply comes from burning of fossil fuels, such as coal, gas and oil, a percentage which is not expected to fall at all. And therein lays the problem with the ever increasing demand for energy and the corresponding environmental problems generated by burning fossil fuels. Generating energy without polluting the environment has become a real challenge. Renewable energy, including solar, are more than ever needed to counter the steady warming of the earth's surface.

Using sunlight to produce energy appears as one of the most sustainable energy solutions. Indeed, the sun illuminates the earth with a large amount of energy: one hour of sunlight could in principle provide the yearly energy consumption of our world today.[2] However sunlight is dispersed hence needs to be captured and converted to other forms of energy such as electrical or chemical to be useful. This conversion is already realized by Nature itself via the photosynthesis carried out by green plants. In the photosynthesis, a photon is absorbed and its energy is converted into chemical energy via a complex series of electron and energy transfer processes. Thus Nature could be an excellent source of inspiration. Understanding the natural processes is of crucial importance to develop artificial photosynthetic systems using man-made materials. Over the years, much work has been carried out to build simple model systems that could mimic Nature in order to get a better understanding of the photoinduced electron transfer processes involved in the photosynthesis.[3-12] A vast variety of donor-acceptor systems have been investigated with the primary aim to create long-lived charge-separated states whose energy could be further use to drive secondary redox reactions.[13-23]

Another field that could benefit from the knowledge gained by exploring the natural photosynthesis is molecular electronics, where molecules are proposed to replace components in today's electronics, such as transistors, rectifiers and switches to name a few.[24-26] Using molecules as components to form nanometer scale electronic circuits is one of the promising approaches to overcome the limitation of the continuous shrinkages of the sizes in silicon-based semiconductor manufacturing.[27] Over the last thirty years, a large variety of organic functional molecules have been explored and proposed as wires, rectifiers or memories and switches.[28] In particular molecular wires have been extensively investigated. Here the motivation is different from the artificial photosynthesis field and most studies aim at learning about the ability of molecules to transfer charge over long distances (nanometers) and the ability of controlling this charge transport by determining influencing factors such as driving force and electronic coupling. Recently, porphyrin macrocycles have been proposed as building blocks for molecular wires and have shown interesting photophysical properties with

promising potential for many applications, such as artificial photosynthetic devices,[29] molecular devices[30] and as novel materials in optics.[31]

This Thesis focuses on porphyrin-based molecular wires consisting of zinc porphyrin macrocycles linked at their meso-positions by butadyine units, denoted $\mathbf{P_n}$ (n=1-4, 6, 8). An important property of these conjugated porphyrin oligomers is the conformational flexibility of their backbone. Controlling this conformational flexibility and the organization of these molecular systems is crucial for any future applications in order to obtain the desired photophysical properties and has been the main focus of the work presented in this Thesis. Paper I explores the ability of these molecular systems to self-assemble into organized constructs. At low temperature the studied linear conjugated porphyrin oligomers spontaneously form well-ordered planar aggregates providing thus new interesting systems for electron migration studies. Paper II provides two other routes to control the conformational flexibility of long oligomers $\mathbf{P_n}$ (n=4, 6) and ultimately to control the rate for charge separation in fullerene-appended porphyrin oligomers $\mathbf{P_n}C_{60}$ (n=4, 6) with the porphyrin oligomers as electron donor and a fullerene as the electron acceptor. First, it shows how conformation of long oligomers can be controlled optically and how this can be used to tune the rate of electron transfer. In a second approach coordination of long porphyrin oligomers to an axial ligand is proposed as a chemical way to restrain the conformational flexibility of the systems. Semi-circular complexes $\mathbf{P_n}C_{60}$-$\mathbf{T_8}$ (n=4, 6) are formed in presence of an octadentate ligand $\mathbf{T_8}$ and show a slow rate constant for charge separation. The difference in the charge-separation rate constants observed in the systems $\mathbf{P_n}C_{60}$ and $\mathbf{P_n}C_{60}$-$\mathbf{T_8}$ are attributed to variation of the driving force for charge separation with the excited conformation.

2. Theory

This chapter provides the basic concepts of photophysics as well as the useful theoretical framework for understanding electron transfer reactions based on the work of Marcus,[32] Hush[33] and Levich.[34] The major factors that control electron transfer are introduced, namely the thermodynamic driving force, the reorganization energy and the electronic coupling.

Photophysics

Photophysics describes the interaction between light and matter, one of the most fundamental processes in Physics. In our daily life, we continuously encounter the effects of these interactions; they determine the appearance of everything around us, such as the color of the plants. In this Thesis, all processes and reactions discussed are related to interactions between light and matter.

To describe this interaction, the double nature, generally named the wave-particle duality of light has to be considered. Light can act either like a wave or like a flow of energy particles. In the first definition, light is described as electromagnetic radiation that contains as its name implies an electric and a magnetic component propagating both in time and space. These fields oscillate sinusoidally in directions perpendicular to each other and to the direction of propagation. However light energy is not continuous and thus light has to be treated as particles called photons, whose energy *E* is directly proportional to the frequency of the electromagnetic wave according to Equation 2.1.

$$E = h\nu = \frac{hc}{\lambda} \tag{2.1}$$

where ν and λ are the frequency and the wavelength of the light respectively, h is the Planck's constant, and c the speed of light.[35]

As molecules consist of charged particles, the interaction of light with matter is typically through its electrical component. The electric field of light can induce oscillations in the electron cloud surrounding the atoms. This interaction may result in a rearrangement of the charge distribution in the molecule leading to a different electronic state of the molecule. This phenomenon is commonly known as absorption and upon absorption the molecule moves to an excited state. For absorption to occur, the wavelength and the polarization of the incoming light should be in resonance with the energy levels and the transition dipole moments, respectively, of the molecule. The former condition refers to the Bohr frequency condition, and is generally illustrated by Equation 2.2 in which the energy of a photon is transferred to the molecule bringing it to an excited electronic state.

$$\Delta E = E_f - E_i = h\nu = \frac{hc}{\lambda} \tag{2.2}$$

The strength of this transition depends on the probability of the molecule to be excited, which is described by the effect of the electric dipole moment operator $\hat{\mu}_{fi}$ on the electronic wave functions of the initial ψ_i and final ψ_f states according to Equation 2.3.

$$\vec{\mu}_{fi} = \int \psi_f^* \hat{\mu} \psi_i d\tau \tag{2.3}$$

The probability of transition, i.e. of the incoming light to induce a transition between two states is proportional to the magnitude and the relative orientation of $\vec{\mu}$ and the polarization direction of the incoming light.[35] Thus if one considers θ the angle between the transition dipole and the incoming light, the absorbance A can be calculated as

$$A \propto \left|\vec{\mu}_{fi}\right|^2 \cos\ ^2\theta \tag{2.4}$$

In practice the probability of transition can be directly related to the molar absorption coefficient, ($M^{-1}cm^{-1}$), which is a measurable property of any molecule translating the wavelength or frequency dependence of its absorption spectrum, as illustrated in Equation 2.5.

$$\int \varepsilon(\tilde{\nu}) d\tilde{\nu} \propto \tilde{\nu}_{if} \left|\vec{\mu}_{fi}\right|^2 \tag{2.5}$$

where $\tilde{\nu}_{if}$ is the average wavenumber of the absorption.

Upon absorption, the molecule is moved to an electronically excited state that typically has the same spin multiplicity as the ground state. For most molecules these excited states are generally singlet states where all electronic spins are paired. There are different excited states associated with a molecule, respectively the first S_1, second S_2, third S_3 singlet excited states and so on. Associated to each of these electronic states are also more closely spaced levels, called vibrational and rotational levels. Once in the excited state, there are several pathways for a molecule to lose its energy and return to the ground state S_0. The different deactivation pathways are often illustrated in an energy diagram, commonly known as Jablonski diagram (Figure 2.1).[36] If a higher vibrational level is populated, a rapid vibrational relaxation (VR) to the lowest vibrational level of the singlet excited state occurs first and energy is lost through collisions with the surrounding molecules or the solvent without emission of a photon. From the lowest vibrational level of the singlet excited state S_1, the excess of energy can then be released via different competing pathways often classified in non-radiative and radiative processes. The first possibility is by emission of a photon and refers to fluorescence. In competition with this radiative process, non-radiative processes can occur such as Internal Conversion (IC) and Intersystem Crossing (ISC). Internal Conversion (IC) moves the molecule to a vibronically excited state of the ground state without energy losses. Once in the S_0 state, the excess of energy is again released as heat through vibrational relaxation (VR) to the lowest vibrational level. However in the singlet excited state, a molecule can also spin flip its electron and thus move to a triplet excited state. This process refers to Inter System

Crossing (ISC). From the triplet state the energy can be released through emission of a photon. Since moving a singlet to a triplet state is quantum mechanically forbidden, triplet emission called phosphorescence is less probable and occurs generally on a different time scale than fluorescence (typically lifetimes in the ns regime) with lifetime of μs, ms or longer. Another deactivation pathway can involve the transfer of an electron or a charge in the excited state to a suitable electron acceptor. In the donor-acceptor system $\mathbf{P_n}C_{60}$ studied in this Thesis, the excess of energy in the excited state results in the transfer of an electron from the porphyrin excited state $\mathbf{P_n}^{*}C_{60}$ to the fullerene C_{60} and the molecule moves to a charge-separated state $\mathbf{P_n}^{\cdot-}C_{60}^{+}$.

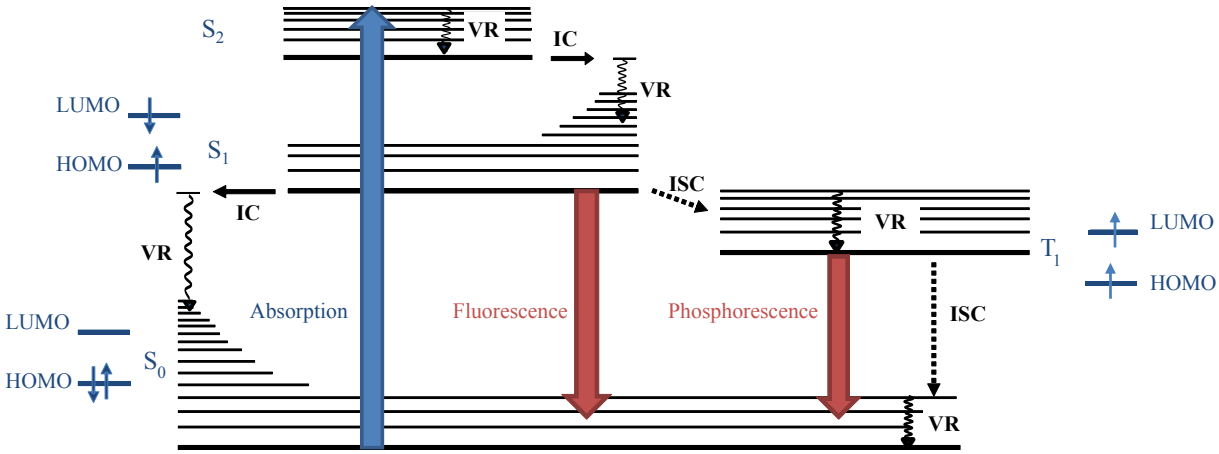

Figure 2.1. A Jablonski diagram. VR corresponds to Vibrational Relaxation, IC to Internal Convertion and ISC to InterSystem Crossing**.**

Associated with each deactivation process is a rate constant k_i whose magnitude reflects the probability of the system to follow this way. Commonly used is also the fluorescence quantum yield ϕ_f of a chromophore defined as the ratio of the fluorescence rate constant and the sum of all rate constants originating from the same state. The fluorescence lifetime τ_f of a molecule corresponds to the average amount of time this molecule remains in the excited state, and can be simply expressed as the inverse of the sum of the rate constants of the deactivation paths (Equation 2.6) often divided into non-radiative and radiative (fluorescence) processes.

$$\tau_f = \frac{1}{k_f + k_{nr}} \tag{2.6}$$

$$\phi_f = \frac{k_f}{k_f + k_{nr}} \tag{2.7}$$

$$k_f = \frac{\phi_f}{\tau_f} \tag{2.8}$$

where k_f is the fluorescence rate constant, k_{nr} is the rate constant of all non-radiative processes, ϕ_f is the fluorescence quantum yield. In presence of an electron acceptor, photoinduced electron transfer can occur and an electron typically moves from the first singlet excited state S_1 to the acceptor state with a rate constant k_{ET}. Hence the sum of the rate constants in Equation 2.6 will increase that result in a shorter fluorescence lifetime.

Electron Transfer Theory

All electron transfer reactions presented in this Thesis are intramolecular photoinduced electron transfer (PET) reactions in which either the donor D or the acceptor A are in the excited state. Indeed photo-excitation increases the energy of the molecule providing thus a driving force for electron transfer between parts of the molecule. Intramolecular photoinduced electron transfer between a donor in the excited state D* and an acceptor A can be represented by the following equation 2.9 with k_{ET} the electron transfer rate constant.

$$D|A \xrightarrow{h\nu} D^*|A \xrightarrow{k_{ET}} D^+|A^- \tag{2.9}$$

Electron transfer processes are typically well described by the Marcus Theory.[32] A common way to discuss electron transfer process is by introducing the potential energy surfaces of a donor-acceptor system D|A shown in Figure 2.2 as function of its reaction coordinate which corresponds to the nuclear and the solvent configuration of the system.

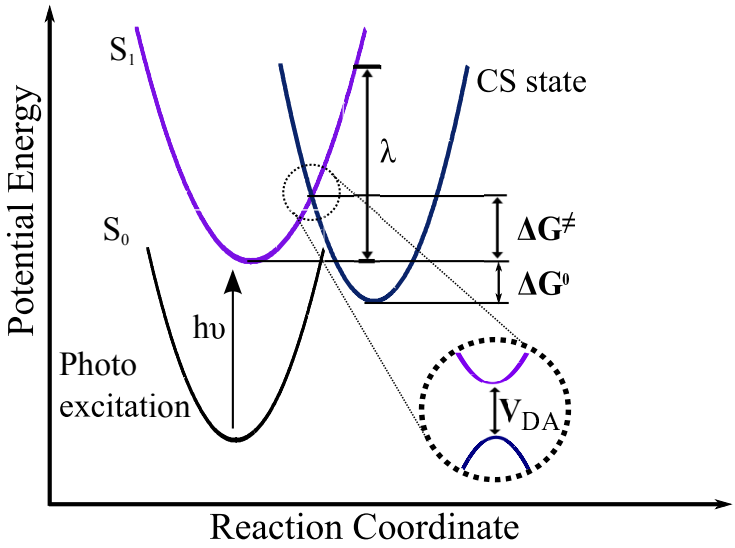

Figure 2.2. Schematic of the potential energy surfaces of the initial state and the charge-separated state showing the factors governing electron transfer processes: the driving force ΔG^0, the activation energy $\Delta G^{\neq}$, the reorganization energy λ and the electronic coupling V_{DA}.

Upon photo-excitation, the molecule moves from the ground-state S_0 to the first singlet excited state S_1, and thereafter can move to a charge-separated state via electron transfer if

there is a sufficient driving force. According to the classical Marcus Theory, electron transfer can only occur at the crossing point between the potential energy surfaces of the excited state S_1 and the charge-separated state CS, named the transition state TS. In other words, this means that for electron transfer to occur, the reactant state (D*|A) should first distort along the reaction coordinate from its equilibrium position to the transition state. This requires an activation energy denoted $\Delta G^{\neq}$. When the system moves from the reactant state D*|A to the product state $D^+|A^-$, it also involves a change in the reaction coordinate: solvent molecules surrounding the charge-separated state $D^+|A^-$ need to spatially reorganize and bond length changes can occur. This again requires energy that is represented by the reorganization energy λ defined as the energy to move the initial reactant state to the same nuclear configuration as the lowest level of the product state. Thus, in the classical Marcus Theory,[32,37-39] the rate constant for electron transfer is given by a standard Arrhenius relationship between the rate constant k_{ET} and the activation energy $\Delta G^{\neq}$.

$$k_{ET} = \kappa_{el}\nu_n \exp\left(\frac{-\Delta G^{\neq}}{k_B T}\right) = \kappa_{el}\nu_n \exp\left(\frac{-(\Delta G^0 + \lambda)^2}{4\lambda k_B T}\right) \quad (2.10)$$

where κ_{el} is the electronic transmission coefficient and ν_n is the frequency of passage through the transition state. ΔG^0 represents the driving force of the electron transfer process and corresponds to the energy difference between the lowest level of the excited state (reactant) and the lowest level of the charge-separated state. Generally the Marcus theory works well for adiabatic electron transfer reactions ($\kappa_{el} \simeq 1$). However for $\kappa_{el} \ll 1$, a quantum mechanical approach to the nuclear motion is needed. This is done by introducing another parameter, the electronic coupling V_{DA} that reflects how easily the donor and the acceptor communicate during the electron transfer. This electronic coupling arises from the overlap of the electronic and vibrational wave functions of the excited state D*|A and the charge-separated state $D^+|A^-$. In Figure 2.4, the electronic coupling represents the energy difference induced by the splitting of the potential energy surfaces of the reactant and the product at the transition state. Taking into account quantum mechanical corrections to the classical Marcus Theory, the rate of electron transfer is given by:

$$k_{ET} = \frac{2\pi}{\hbar}|V_{DA}|^2 \frac{1}{\sqrt{4\pi\lambda k_B T}} \exp\left(\frac{-(\Delta G^0 + \lambda)^2}{4\lambda k_B T}\right) \quad (2.11)$$

The driving force

Just like for any reaction to take place, the molecule needs to lose energy for electron transfer (ET) to occur. This means that the driving force ΔG^0 associated with the ET reaction needs to be lower than zero. The driving force or the difference in energy between the D*|A state and the charge-separated state $D^+|A^-$ can generally be estimated from the oxidation potential of the donor E_{ox} and the reduction potential of the acceptor E_{red} as well as the energy of the 0-0 transition E_{00} of the donor using the Weller equation,[40] Equation 2.12.

$$\Delta G^0 = e(E_{ox} - E_{red}) - E_{00} - \frac{e^2}{4\pi\varepsilon_0 r_{DA}} + \frac{e^2}{4\pi\varepsilon_0}\left(\frac{1}{\varepsilon_s} - \frac{1}{\varepsilon_s^{ref}}\right)\left(\frac{1}{2r_D} + \frac{1}{2r_A}\right) \quad (2.12)$$

In this expression the third term represents the coulombic stabilization and the last term is a correction term related to solvents with ε_s the dielectric constant of the solvent used in spectroscopy measurements and ε_s^{ref} the dielectric constant of the solvent used in electrochemistry measurements. The oxidation and reduction potentials are often measured by cyclic voltammetry. In case of ET from the first singlet excited state S_1, an estimation of the energy of the state E_{00} can be obtained from the wavelength corresponding to the intersection of the normalized absorption and fluorescence spectra.

Depending of the value of the driving force ΔG^0 relative to the reorganization energy λ, different ET regimes can be distinguished: the normal region and the inverted region. In the normal region ($|\Delta G^0| < \lambda$), according to Equation 2.10, as the driving force ΔG^0 increases, the activation energy $\Delta G^{\neq}$ decreases, resulting in a faster electron transfer rate constant k_{ET}. In contrast in the so-called Marcus inverted region ($|\Delta G^0| > \lambda$), when ΔG^0 becomes more negative, the activation energy $\Delta G^{\neq}$ increases again and the electron transfer process is slowed down. The different ET regimes are illustrated in Figure 2.3.

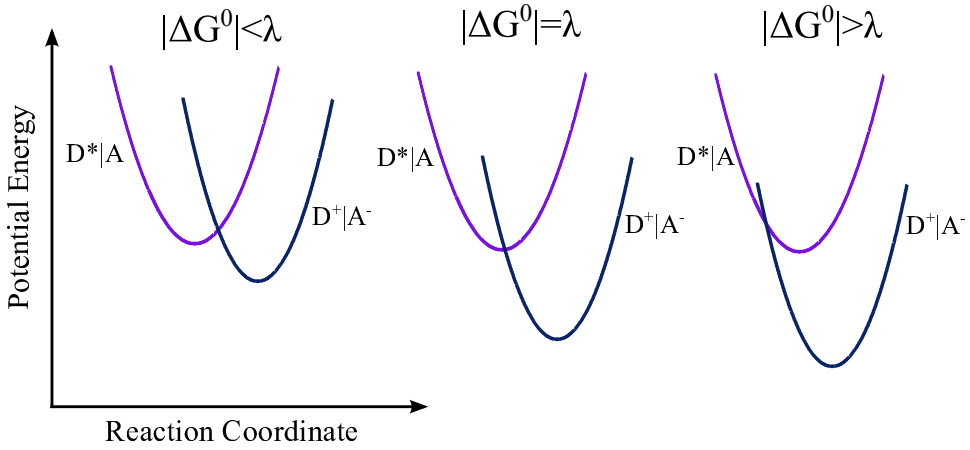

Figure 2.3. Schematic of the state energy diagrams corresponding to the different ET regimes.

The reorganization energy

The reorganization energy λ contains two parts as illustrated in Equation 2.13:

$$\lambda = \lambda_{in} + \lambda_{out} \quad (2.13)$$

The inner part λ_{in} represents the distortion of the nuclear configuration, such as changes in bond lengths that the donor-acceptor system undergoes when moving from the reactant state to the product state. The outer part λ_{out} is generally called the solvent reorganizational

energy. It originates from the polarization reorientation of the solvent molecules surrounding the system D|A when electron transfer occurs. While λ_{in} could be generally obtained from quantum mechanical calculations,[41] the solvent reorganizational energy λ_{out} can be estimated from Equation 2.14 approximating the donor and acceptor as spheres.[42]

$$\lambda_{out} = \frac{e^2}{4\pi\varepsilon_0}\left(\frac{1}{2r_D} + \frac{1}{2r_A} - \frac{1}{r_{DA}}\right)\left(\frac{1}{n^2} - \frac{1}{\varepsilon_s}\right) \tag{2.14}$$

Where r_D and r_A are the radii of the donor and acceptor respectively, r_{DA} is their center-to-center distance, and n and ε_s are solvent parameters, its refractive index and its dielectric constant respectively.

The electronic coupling

The electronic coupling V_{DA} can be defined by

$$V_{DA} = \langle \psi^0_{D^*A} | \hat{H}_{el} | \psi^0_{D^+A^-} \rangle \tag{2.15}$$

where $\psi^0_{D^*A}$ and $\psi^0_{D^+A^-}$ are the electronic wave functions of the excited state and the charge-separated state respectively, and $\hat{H}_{el}$ is the Born Oppenheimer electronic Hamiltonian for the system. Depending of the value of V_{DA}, two types of electron transfer reactions are distinguished: adiabatic ET reactions for relatively large V_{DA} and non-adiabatic ET reactions for small values of V_{DA}. As shown in Figure 2.4 for adiabatic ET reactions at the transition state, the system always moves on the lowest potential energy surface hence the probability of ET to occur is close to 1, every time the system reaches the transition state. In contrast, for non-adiabatic reactions, the system remains moving on the reactant potential energy surface oscillating between the transition state and its equilibrium position. It is only occasionally that it will pass through the transition state and charge separation will occur.

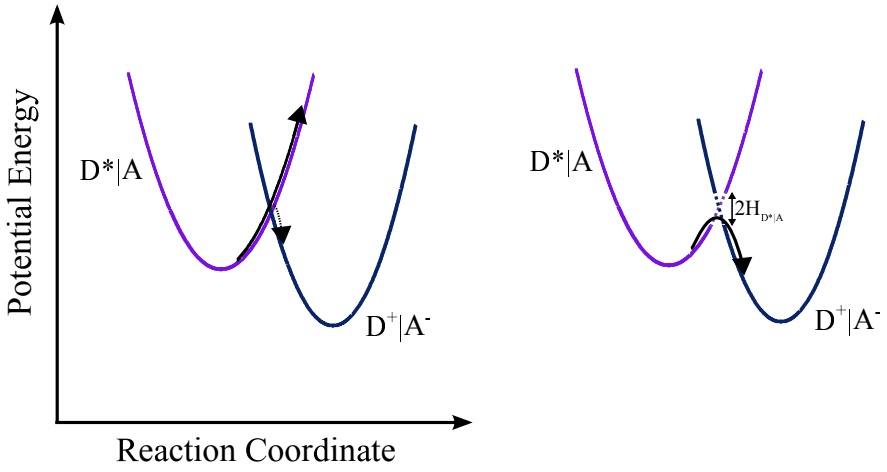

Figure 2.4. Adiabatic (**left**) and nonadiabatic (**right**) electron transfer. $H_{D^*|A}$ represents the electronic coupling.

3. Porphyrin Molecular Systems inspired by Nature

This chapter gives first a brief description of the natural photosynthesis with an emphasis on the role of electron transfer in these processes. Then the main concepts used for the development of artificial photosynthetic devices are summarized. Thereafter the porphyrin moieties incorporated in the studied system are introduced. Finally the conjugated porphyrin oligomers studied in this Thesis are presented, together with the appended-fullerene porphyrin systems.

Natural Photosynthesis versus Artificial Photosynthesis

In the natural photosynthesis, conversion of light into chemical energy occurs via a series of step-wise electron transfer processes to create sufficient energy for water splitting and carbon dioxide reduction.[43] A simplified schematic of the overall process, known as "Z-scheme" is given in Figure 3.1.

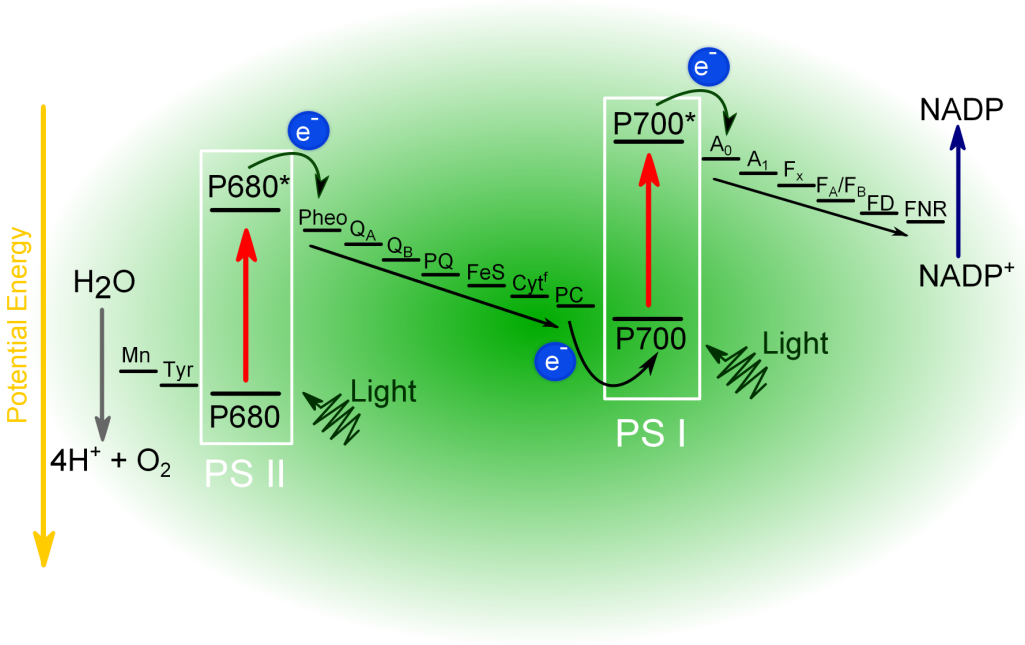

Figure 3.1. Simplified schematic of the charge-separation processes in the natural photosynthesis. P680: pigment (chlorophyll) absorbing at 680 nm; P700: pigment (chlorophyll) absorbing at 780 nm; Mn: manganese calcium oxide cluster; Tyr: tyrosine; Pheo: Pheophytin; Q_A: primary plastoquinone electron acceptor; Q_B: secondary plastoquinone electron acceptor; PQ: plastoquinone; FeS: iron sulphur protein; Cyt^f: cytochrome f; PC: plastocyanin; A_0: primary electron acceptor of PSI; A_1:phylloquinone; F_x, F_A, F_B: three separate iron sulphur centers; FD: ferrodoxin; FNR: nicotinamide adenine dinucleotide phosphate reductase.

As depicted in Figure 3.1 the natural photosynthesis starts with the absorption of two photons by photosynthetic systems PSI and PSII that consist of an assembly of chlorophylls (antennas) absorbing light in the visible region. Light absorption is then followed by a series of downhill electron transfer steps to generate high energy intermediates. In more details, light absorption at PSII pumps electrons to a higher electronic state yielding to P680*, while light absorption at PSI creates P700* which then transfers an electron to A_0 the primary acceptor of PSI. P680* further transfers an electron to the oxidized $P700^+$ via a series of electron-transfer steps starting with the reduction of Pheophytin. Following this first electron transfer, $P680^+$ can oxidize tyrosine that subsequently oxidizes a manganese calcium oxide cluster. Thus this series of subsequent electron-transfer processes allows moving away the electron from the initial acceptor, creating a charge-separated state with a long enough lifetime to carry on with the light-independent ("dark") reactions of photosynthesis. For oxygenic photosynthetic systems, the "dark" reactions of photosynthesis refer to the oxidation of water into molecular oxygen and protons in PSII, while the products of the light-induced reactions (ATP and NADPH) are used in the reduction of carbon dioxide to carbohydrate or other kinds of energy.

However the energy-conversion efficiency of the overall natural photosynthesis is only in the range of few percentages.[44] For potential use as source of energy the photosynthesis needs to be better. Thus artificial photosynthesis has been proposed as biomimetic approach to the natural photosynthesis. Simpler systems are designed to mimic the reaction features of the natural photosynthesis and ultimately achieve better results than the natural photosynthesis. Using Nature as a source of inspiration, a primary requirement for artificial photosynthetic devices is an electron donor that absorbs efficiently in the visible region and a suitable electron acceptor. First artificial photosynthetic systems were based on a porphyrin (P) as electron donor covalently linked to a quinone (Q) as electron acceptor in which excitation of the porphyrin yields to the charge-separated state P^+-Q^-.[19,45-47] However these charge-separated states had lifetimes of ~100 ps, too short to use their energy to carry on chemical reactions. The main strategy adopted to prolong the lifetime of these charge-separated states has been the use of additional donors and acceptors that enables to spatially separate the electrons and reduce the electronic coupling between the two radical ions.[14-22] The first donor-acceptor triad system proposed by Gust et al. was a carotenoid-porphyrin-quinone triad (C-P-Q) in which the primary charge-separated state C-P^+-Q^- undergoes charge-shift to form a final charge-separated state C^+-P-Q^- with a lifetime of hundreds of ns.[48] Over the years, several studies have investigated photo-induced electron transfer using designed donor-acceptor model systems to learn about the influence of the structure on the electron transfer. [14-22] In this Thesis, the initial charge separation step is investigated in a simple dyad system, fullerene-appended porphyrin oligomer $\mathbf{P_n}C_{60}$ (n=4, 6) in which electron transfer is strongly influenced by the conformational disorder of the oligomer.

Porphyrins

Porphyrins are heterocyclic macrocycles consisting of four pyrrole units. Porphyrins and their derivatives appear naturally in many biological systems such as chlorophylls and hemoglobin in which they play an essential role. As an example in the natural photosynthesis, porphyrin-like chlorophylls act as sun light harvester. However chlorophylls are rather complex to synthesize, and hence simpler model systems based on the porphyrin unit as building block have been used for electron and energy transfer studies.

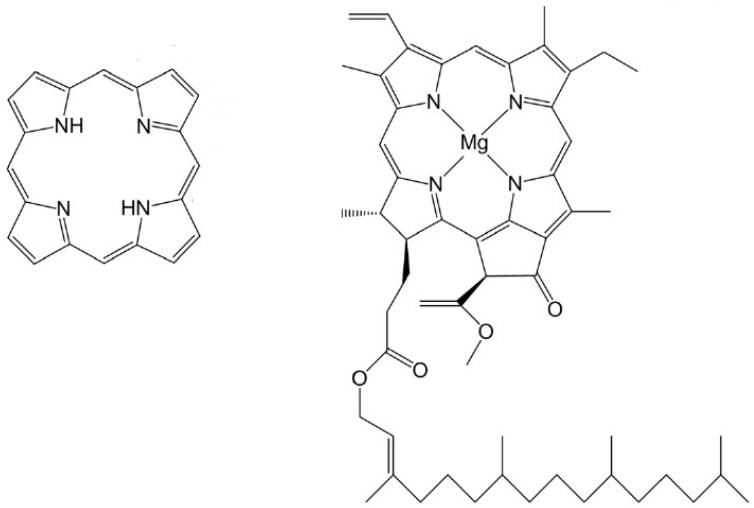

Figure 3.2. Molecular structure of (**left**) a free-base porphyrin and (**right**) chlorophyll a.

The free-base porphyrin as shown in Figure 3.2 has no central atom, but insertion of a metal cation is generally rather easy. A wide range of metal cations can coordinate to the porphyrin free-base that allows one to tune their redox potentials and photophysical properties. Porphyrins have electronic transitions in the visible region of the electromagnetic spectrum and their absorption spectra (Figure 3.3) are characterized by a strong transition to the second excited state ($S_0 \rightarrow S_2$) around 400 nm called the Soret band and a less intense transition to the first excited state ($S_0 \rightarrow S_1$) at about 600 nm called the Q band. The absorption spectra of porphyrins can be well explained by the Gouterman four orbital model that considers the four frontier orbitals (HOMO, HOMO-1 and two degenerate LUMO orbitals).[49] When considering a D_{4h} symmetric metalloporphyrin, the two lowest unoccupied orbitals e_g are degenerate, while the two highest occupied orbitals a_{1u}, a_{2u} are almost degenerate. Orbital mixing gives rise to two doubly degenerate transitions: a high energy transition with a greater oscillator strength (Soret band) and a low energy transition with a smaller oscillator strength (Q band) as depicted in Figure 3.3.

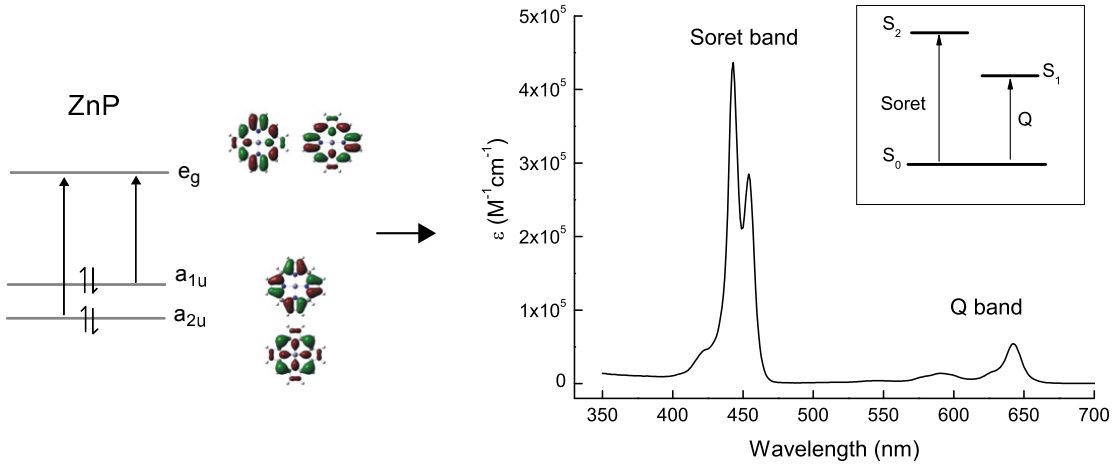

Figure 3.3. (**left**) The four frontier orbitals of metalloporphyrins taken into account in the Gouterman model and (**right**) the resulting electronic spectrum.

Insertion of a metal center generally affects the relative energies and intensities of these transitions. In particular metals of d^m m = 6-9 that have partially filled dπ orbitals interact significantly with the electrons of the porphyrin resulting generally in a blue-shift of the absorption spectrum. In contrast porphyrins that contain closed-shell metal cations (d^{10}) such as Zn^{2+} perturb very little the electronic structure of the porphyrin. Hence zinc porphyrin show absorption spectra similar to the free-base porphyrin spectrum (Figure 3.3). Also zinc porphyrins present the advantage of being more stable than Mg, Cd or Pb porphyrins in which accidental demetallation is relatively current. The solubility of zinc porphyrins can also be improved by the use of solvents such as THF or additives such as pyridine that can coordinate to Zn centers.

The Donor-Acceptor Systems Studied

Using conjugated motifs as linkers, several porphyrin units can be assembled together to form conjugated porphyrin oligomers that can act as molecular wires. Over the last 40 years, different porphyrin-based molecular wires that mostly differ by the type of linkers have been synthesized and investigated, mainly by the groups of Crossley,[50] Anderson,[31,51] Therien,[29,52] and Osuka.[53,54] The general structures of some porphyrin-based molecular wires are shown in Figure 3.4. In all the structures, the nature of the linkers chosen determine the distribution of porphyrin-porphyrin dihedral angles, and hence the electronic coupling between neighboring units as well as the extent of conjugation.

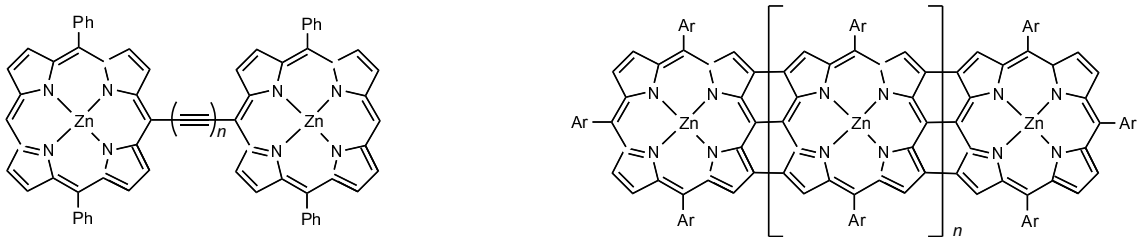

Figure 3.4. Molecular structure of (**left**) meso-butadiyne-linked zinc dimers developed by Therien et al.[29] and (**right**) meso-meso and β-β triply-linked porphyrin arrays developed by Osuka et al.[54]

In this work, the studied molecules are butadiyne-linked porphyrin oligomers, denoted $\mathbf{P_n}$, ranging from the monomer to the octamer (Figure 3.5). At the meso-positions of the porphyrin unit, aryl side chains were connected to improve the solubility of the oligomers in organic solvents and prevent their aggregation.

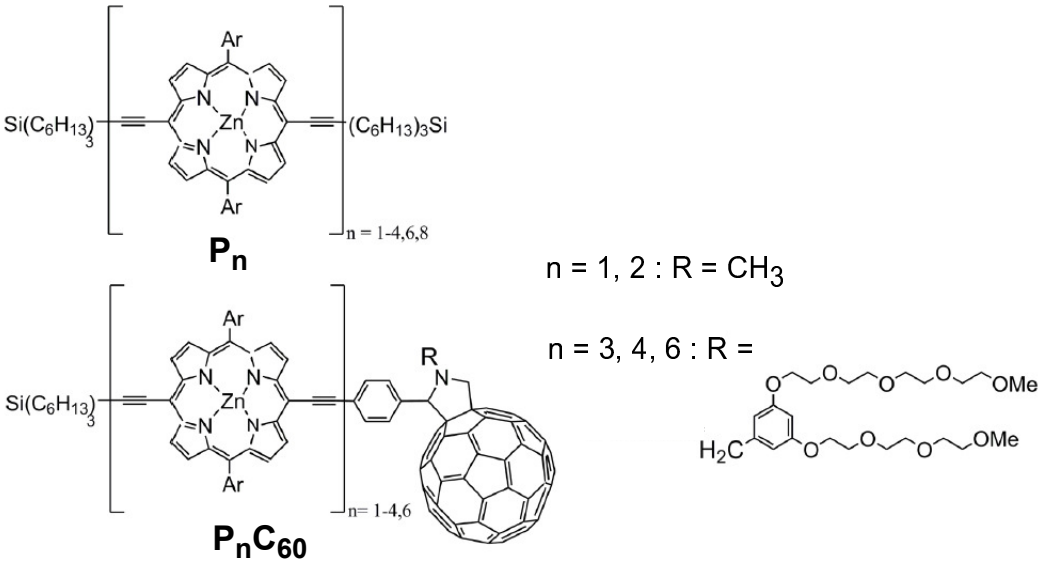

Figure 3.5. Molecular structure of the porphyrin oligomers $\mathbf{P_n}$ and the fullerene-appended dyad $\mathbf{P_n}C_{60}$ studied in this work. The aryl substituents, Ar, are 3,5-di(t-butyl)phenyl for n=1 and 3,5-di(octyloxy)phenyl for n = 2-8.

As mentioned in the introduction, an important aspect of these porphyrin oligomers is their conformational flexibility. At room temperature, butadiyne linkers allow an almost barrierless rotation of the individual porphyrin units. This almost free rotation of the porphyrin moieties results in a wide distribution of conformers differing only by their porphyrin-porphyrin dihedral angle. Thus the ground-state absorption spectra of these oligomers $\mathbf{P_n}$ (n = 1-8) provided in Figure 3.6 is an average of the different conformations present. As the oligomer gets longer, the number of possible conformers increases resulting in a broader and less structured Q band. The influence of conformational disorder on the photophysical properties of these oligomers has already been thoroughly investigated for the

dimer $\mathbf{P_2}$, both experimentally and via quantum mechanical calculations.[55] Two limiting spectroscopic species were identified, namely a planar and twisted conformers, that could be selectively excited. In the excited state twisted conformations tend to relax almost quantitatively to planar conformations before emitting and returning to the ground state. In this work, the conformational dependence of the spectral properties of these oligomers $\mathbf{P_n}$ (n = 1-8) has been further studied as function of the temperature (Paper I).

From these porphyrin oligomers $\mathbf{P_n}$, model systems for charge separation devices such as bulk-heterojunction solar cells can be built by appending a fullerene as electron acceptor to the oligomer chain (Figure 3.5). Besides the significant popularity of fullerenes as electron acceptors in donor-acceptor systems since reported by Gust et al.,[56] the use of Buckminsterfullerene C_{60} as electron acceptor presents several advantages. First its reduction potential makes the photo-induced charge separation thermodynamically favorable for any porphyrin oligomer length. Secondly, experimentally C_{60} absorbs mainly in the UV region while the radical anion C_{60}^{-} shows relatively strong bands in the near IR and hence its formation and decay can be followed in transient absorption measurements. As for the oligomer chains $\mathbf{P_n}$, the spectroscopic and electronic communication in fullerene appended porphyrins $\mathbf{P_n}C_{60}$ is strongly governed by their conformational flexibility. A recent study on the short dyad $\mathbf{P_2}C_{60}$ reported an electron transfer rate from twisted conformations 4 times higher than for planar conformers,[57] attributed mainly to the stronger electronic coupling to the C_{60} in the twisted conformation. The temperature dependence of the electron transfer from the oligomer chain to the fullerene has also been explored for the entire series $\mathbf{P_n}C_{60}$ (n=1-4, 6).[58] The charge separation reaction was found to occur in two steps with first the migration of the excitation energy along the oligomer chain followed then by direct charge separation. In the work presented in Paper II, the conformational dependence of the charge separation step in the longest oligomers $\mathbf{P_n}C_{60}$ (n=4, 6) has been further investigated, either by optically exciting different conformations or by chemically modulating the conformation of the porphyrin chain via ligand coordination.

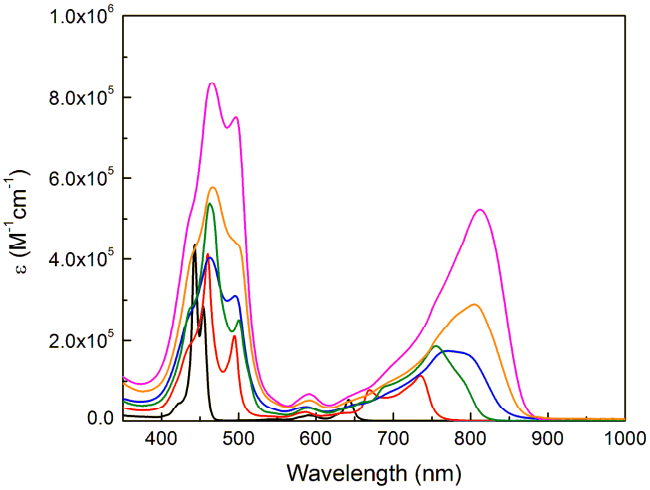

Figure 3.6. Molar absorptivity of butadiyne-linked porphyrin oligomers: $\mathbf{P_1}$ (black), $\mathbf{P_2}$ (red), $\mathbf{P_3}$ (green), $\mathbf{P_4}$ (blue), $\mathbf{P_6}$ (orange) and $\mathbf{P_8}$ (pink).

4. Synopsis

This chapter gives a summary of the results described in Papers I and II together with a description of the main spectroscopic methods used. First the ability of linear conjugated porphyrin oligomers $\boldsymbol{P_n}$ *(n = 1-4, 6, 8) to form well-defined aggregates is demonstrated in Paper I. Then Paper II discusses the conformational dependence of charge-separation in long porphyrin oligomer-fullerene donor-acceptor systems* $\boldsymbol{P_n}C_{60}$ *(n = 4, 6).*

Paper I: Self-Assembly of Linear Porphyrin Oligomers into Well-Defined Aggregates.

Steady-State Methods

In Paper I, two types of spectroscopic steady-state methods, namely absorption and fluorescence emission, have been used. Both techniques use a continuous illumination of the sample, and hence keeping the excited state population constant during the measurement.

Absorption Spectroscopy

Absorption of light by molecules is an easy process to study. Absorption measurements are carried out by letting light passing through a sample and by recording the intensity difference between the incident I_0 and transmitted light I at each wavelength (Figure 4.1).

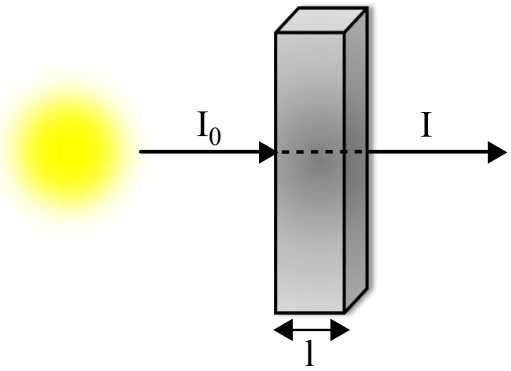

Figure 4.1. Schematic of an absorption measurement

According to Beer-Lambert law,[35] the absorbance A is proportional to the light path l and the concentration of the sample c

$$A(\varepsilon) = log\left(\frac{I_0}{I}\right) = \varepsilon(\tilde{\nu})cl = \varepsilon(\lambda)cl \qquad (4.1)$$

where ε is the molar absorptivity of the molecule ($M^{-1}cm^{-1}$) and is related to the transition probability. Despite its simplicity, this technique can provide lot of information on the electronic structure of a system but also on interactions (electronic coupling) between an acceptor and a donor in donor-acceptor systems. In this paper, absorption spectroscopy has been used to follow the formation of aggregates and quantify the dimerization process occurring between porphyrin oligomers $\mathbf{P_n}$.

Steady-State Emission Spectroscopy

Steady-state emission spectroscopy consists in measuring the emission of absorbed photons by means of a spectrofluormeter. The sample is excited with an intense light source and the emitted photons are collected by a photomultiplier tube in a direction perpendicular to the excitation light. Two types of measurements can be performed: emission and excitation spectrum. Emission spectra are recorded by setting the excitation wavelength and collecting the wavelength dependent emission intensity. In contrast excitation spectra correspond to the dependence of the emission intensity on the excitation wavelength. They are measured by setting the emission monochromator at the desired emission wavelength that is generally the emission maximum. The excitation spectra are then obtained by scanning with the excitation monochromator the absorption bands of the fluorophore.[36] Generally most fluorophores have the shape of their emission spectra independent on the excitation wavelength. As a consequence their excitation spectra are superimposable on their absorption spectra. However in the presence of more than one fluorophore in the sample, this resemblance does not hold anymore. However if the fluorophores have slightly different emission wavelengths, excitation spectra can provide information on the origin of the emission. Depending on the set emission wavelength, the excitation spectrum will resemble the absorption spectrum of one or another species present in the sample. For example in Paper I, excitation spectra were recorded and allowed to determine the origin of the different emission peaks observed to either the porphyrin oligomers $\mathbf{P_n}$ or the formed aggregate.

Steady-state emission spectroscopy can also be used to measure the fluorescence quantum yield ϕ_f of a fluorophore (see section 2). Experimentally the quantum yield of a fluorophore is generally determined with the use of a reference or standard and is calculated according to equation 4.2.

$$\phi_{f,sample} = \phi_{f,ref} \frac{A_{ref}}{A_{sample}} \frac{I_{f,sample}}{I_{f,ref}} \frac{n^2_{sample}}{n^2_{ref}} \tag{4.2}$$

where I_f are the integrated wavenumber emission intensities, A_{ref} and A_{sample} are the absorbance of the reference and the sample at the excitation wavelengths respectively, and n_{ref} and n_{sample} are the refractive indices of the respective solvents. In order for equation 4.2 to be valid the sample absorbance has to be low enough to avoid inner-filter effects.[59]

Comparison of the normalized absorption and emission spectra, and more particularly the Stokes shift, can also provide information on the structure of the fluorophore and its surrounding environment. As shown in the Jablonski diagram (Figure 2.1), emission of most molecules occurs from the first singlet excited state S_1, a state that it is lower in energy than the absorbing state. Thus emission of a fluorophore is typically observed at longer wavelengths than absorption.[60] The Stokes shift associated to a fluorophore is defined as the difference in wavelength between the absorption and emission band. The reason for this Stokes shift is mainly the rapid decay to the lowest vibrational level of S_1 via vibrational relaxation (on the fs to ps time scale) and the decay of the fluorophore to higher vibrational levels of S_0. Thus the Stokes shift is generally sensitive to the fluorophore environment, the solvent polarity and the formation of complexes.

Self-Assembled Porphyrin Oligomers

In this first paper, we have explored how the temperature influences the conformational distribution of linear porphyrin oligomers $\mathbf{P_n}$ (n = 2-4, 6, 8). When lowering the temperature below a certain point, the porphyrin oligomers spontaneously self-assemble into highly-ordered and planar aggregates.

The self-assembly is characterized by dramatic changes in the ground-state absorption spectra of the porphyrins as shown in Figure 4.2 for $\mathbf{P_8}$, $\mathbf{P_6}$ and $\mathbf{P_4}$. As the temperature is decreased, the Q band becomes more structured but more importantly a new red-shifted absorption band is growing in and dominates the spectra below 150 K. This red-shift peak suggests a planarization of the oligomers accompanying the aggregate formation. Previous studies on the dimer $\mathbf{P_2}$ already predicted a red-shift of the Q band for planar conformations.[55] The formation of planar aggregates is also supported by the sharpness of the peak that suggests a reduced distribution of conformers at low temperatures including more or less only planar conformers. In addition comparison of the absorption and emission spectra shows a very small Stokes shift (Figure 4.3). These spectral changes are very similar to the one observed in the formation of J-aggregates. Discovered more than 80 years ago by Scheibe et al.[61-64] and Jelley,[65,66] J-aggregates have already been observed in a variety of dyes including cyanines,[67,68] porphyrins,[69] phtalacyanines[70-72] and perylene bismides.[73,74] These J-aggregates present an unusual optical behavior with sharp and red-shifted absorption band and concomitantly a strong fluorescence with very small Stokes shift. However while J-aggregates are typically large aggregates, here much smaller aggregates, probably a dimer or trimer give rise to similar spectral changes due to planarization effects. The process was also reversible and sensitive to the solvent. The aggregation could be avoided by quick cooling to the liquid nitrogen temperature or with the use of coordinating solvents such as THF or pyridine.

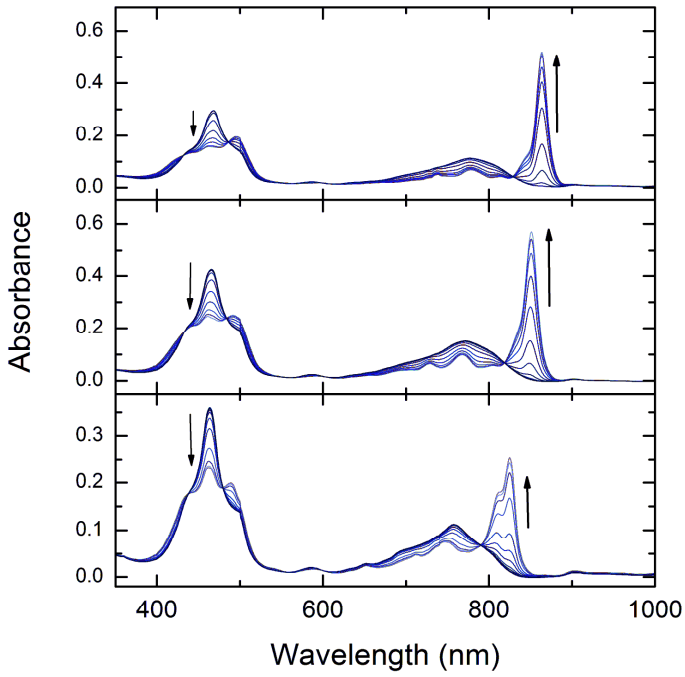

Figure 4.2. Temperature-dependent absorption of $\mathbf{P_8}$ (**upper**), $\mathbf{P_6}$ (**middle**) and $\mathbf{P_4}$ (**lower**) in 2-MTHF. The displayed temperature intervals are 170-150 K for $\mathbf{P_8}$ and $\mathbf{P_6}$ and 165-135 K for $\mathbf{P_4}$. A weak baseline distortion at 900 nm is observed at lower temperature and is attributed to changes in the solvent absorptivity (vibrational overtone absorption).

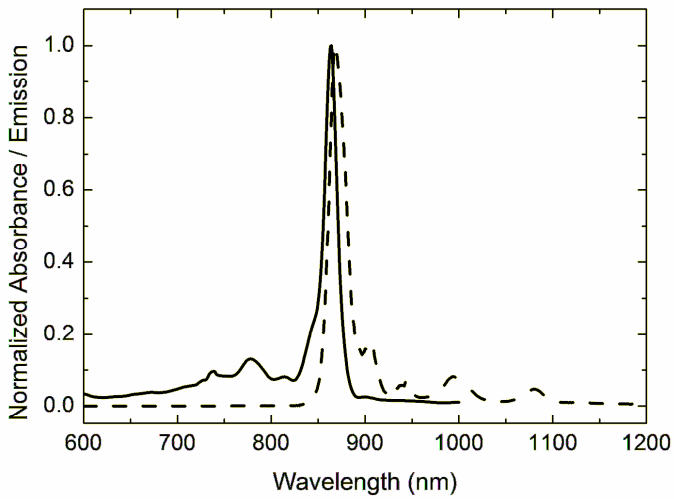

Figure 4.3. Normalized absorption (solid) and emission (dashed) spectra of the octamer $\mathbf{P_8}$ at 150 K. The excitation wavelength was 864 nm.

The absorption spectra in Figure 4.2 also reveal several isobestic points suggesting the presence of two absorbing species in equilibrium. The process could be well described by a two-state model between the free oligomer and the aggregate. Singular Value Decomposition (SVD) was applied to extract the main spectral components. The data were then fitted to a simple equilibrium model in which the apparent enthalpy and entropy changes were

optimized. In particular a dimerization process was considered as including larger constructs did not improve the fitting significantly. The extracted spectral components for the octamer **P_8** are shown in Figure 4.4 along with the concentration profiles of free octamer and aggregates in units of oligomer concentration as function of the temperature. Table 4.1 provides the optimized thermodynamic parameters along with empirically determined melting temperatures. The enthalpy and the entropy changes vary almost proportionally with the oligomer size while the melting temperatures obtained increase with the length of the oligomer. The large negative entropy values confirm the formation of highly ordered aggregates. The value of the aggregation enthalpy increases with around (-)20 kJ/mol per added porphyrin monomer unit in the oligomers. This value can be compared to the value reported by Hunter and Sanders[75,76] who estimated the ππ-stacking enthalpy between two zinc porphyrins to be 48 ± 10 kJ mol^{-1}. The lower value observed here can be explained by the high dependence of the enthalpy changes on the solvent and the interaction between the porphyrins.

Table 4.1. Optimized enthalpy (ΔH) and entropy (ΔS) changes of the porphyrin oligomer dimerization extracted from the fit[a]

	ΔH (kJ/mol)	**ΔS (J/mol K)**	**T_m (K)**
Tetramer	-86	-459	146
Hexamer	-137	-749	158
Octamer	-168	-906	163

[a]T_m is the apparent melting temperatures where 50 % of the oligomers have formed aggregates. The total oligomer concentration is 0.19 μM for **P_4**, 0.48 μM for **P_6** and 0.29 μM for **P_8**.

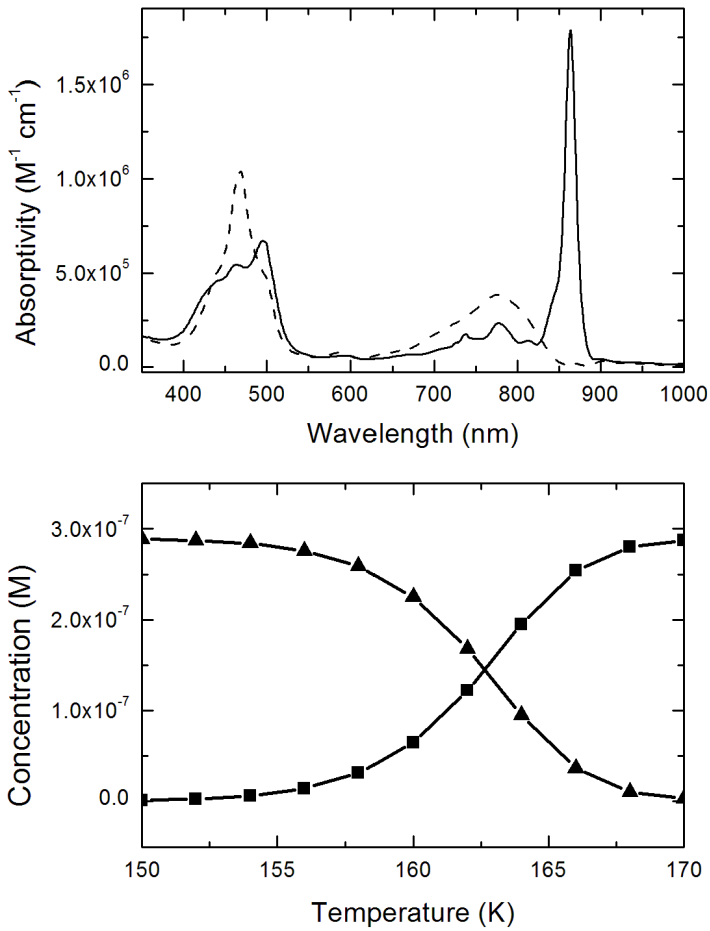

Figure 4.4. (**Top**) The two most significant spectral components extracted from SVD-analysis of the $\mathbf{P_8}$ dimerization and (**Bottom**) the corresponding concentration profiles of the monomer (squares) and the dimer (triangles). The spectral profiles and concentration variations correspond to the optimized enthalpy (ΔH) and entropy (ΔS) values in Table 4.1. The dimer concentration is displayed in units of $\mathbf{P_8}$ concentration.

The kinetics of the dimerization reaction was also investigated. The process was characterized by a slow association rate constant, much slower than the rate constant for a diffusion-limited reaction. Thus the slow rate constant observed could not be explained by the high viscosity of the solvent at low temperature but rather by the importance of having a planar conformation of the oligomer for the dimerization to occur. The large distribution of rotational conformers present in long oligomers such as $\mathbf{P_4}$, $\mathbf{P_6}$ and $\mathbf{P_8}$ greatly slow down the process. Shorter oligomers $\mathbf{P_n}$ ($n \leq 3$) have a narrower distribution of conformers and thus a higher probability of showing a close to planar conformation. However as seen in Table 4.1, the apparent melting temperature decreases with the size of the oligomer, and thus melting temperatures below 140 K can be expected for shorter oligomers $\mathbf{P_n}$ ($n \leq 3$). At such low temperature, the viscosity of the solvent is very high, resulting in extremely slow equilibration rates that prevent any observation of aggregate formation for $\mathbf{P_2}$ and $\mathbf{P_3}$.

As mentioned before, the aggregates observed here are probably small aggregates not larger than dimers or trimers. Although several experiments (resonance light scattering, dynamic light scattering and steady-state anisotropy) were performed to determine the size of these aggregates, no evidence of large aggregates was found. The strongest evidence for the formation of small aggregates came from the comparison of the fluorescence quantum yields of the free oligomer with the aggregate. As shown in Table 4.2, both the free oligomer and the aggregate show very similar radiative rate constants, that suggests transition moments comparable in size. Large aggregates such as J-aggregates generally have huge absorptivities compared to their monomer. Another evidence for small aggregates was given by the aggregation reaction occurring even in presence of pyridine. Aggregates spontaneously formed also in presence of pyridine and this without any change in the melting temperature, but only a red-shift of the absorption spectrum. This red shift was similar to the one observed for the free oligomer when adding pyridine. For large aggregates, only few Zn centers will be accessible to pyridine coordination, and most of the oligomers will not show any change in the transition energies. Finally, systems with appended electron donor and/or acceptor, $\mathbf{P_n}C_{60}$ and Fc$\mathbf{P_n}C_{60}$ could also self-assemble. This self-assembly was accompanied by similar spectral changes as shown in Figure 4.5. This provided another evidence of the formation of small aggregates as it would be difficult for larger constructs to accommodate bulky groups such as the C_{60}. These aggregates with well-defined structures could provide interesting model systems for investigating charge migration in e.g. bulk-heterojunction solar cells.

Table 4.2. Fluorescence quantum yields (Φ_f) and lifetimes (τ_f) and radiative rate constant (k_f) of the porphyrin octamer measured at 163 K where approximately half of the oligomers have converted to aggregates.

Compound	Φ_f[a]	τ_f(ps)[b]	k_f(ns^{-1})
Free octamer	10 %	930	0.107
Aggregate	7 %	575	0.122

[a] Optical density of the two species at the excitation wavelength was scaled with their corresponding absorptivities and their individual emission spectra was obtained by subtracting the contribution from the other species. The quantum yield of $\mathbf{P_6}$ in toluene was used as reference.[77] [b] The sample was excited at 495 nm and the emission decay was measured at 800 nm and 867 nm for the free octamer and aggregates respectively.

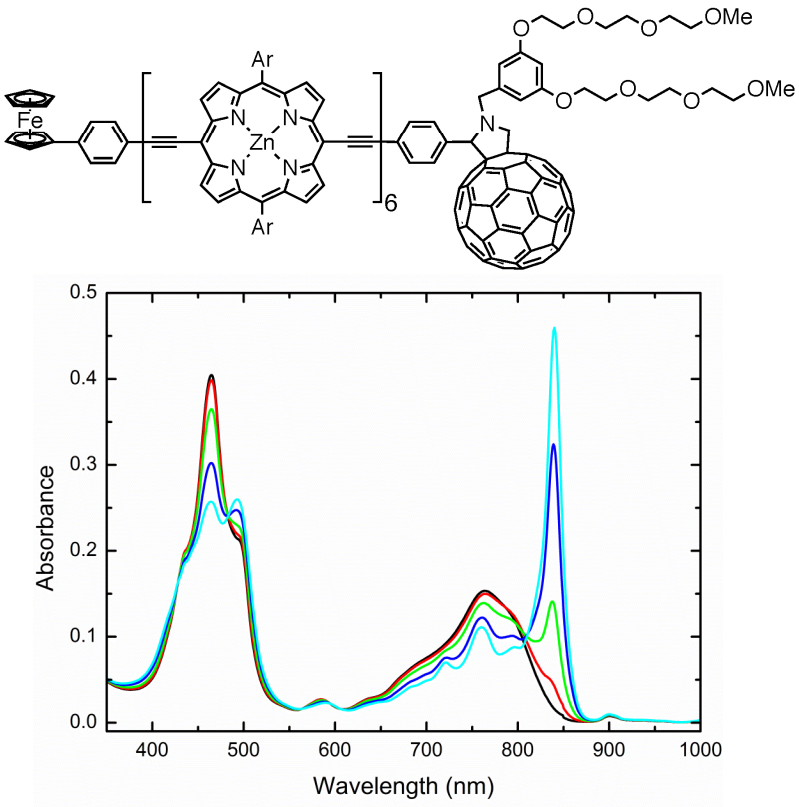

Figure 4.5. (**top**) Molecular structure of the fullerene and ferrocene appended hexamer system, Fc**P**$_6$C$_{60}$; (**bottom**) Absorption spectra of Fc**P**$_6$C$_{60}$ in MTHF measured at 180 K (black), 170 K (red), 166 K (green); 162 K (blue) and 158 K (cyan).

Paper II: Conformational Gating of Charge Separation in Porphyrin Oligomer-Fullerene Systems

Time-resolved Methods

In this paper, in addition to the steady-state methods presented before, a new technique is introduced: time-resolved fluorescence.

Previously we have shown that steady-state fluorescence can provide quantitative information such as the fluorescence quantum yield of a sample. In a donor-acceptor system, a relative fluorescence quantum yield can be determined by comparing the emission of the system in presence and absence of electron acceptor and thus provide information on the efficiency of the electron transfer process. However the emission from any fluorophore contains more information, in particular on the nature of the deactivation processes in the excited state and their kinetics. By measuring the fluorescence decay of a sample, i.e. its fluorescence intensity over time, it is possible to probe conformational changes in the excited state such as planarization processes, but also to determine the rate constants of the different deactivation pathways such as electron transfer in donor-acceptor systems. The techniques that enable one to follow the fluorescence intensity of a sample over time are called time-resolved fluorescence techniques. Compared to the steady-state fluorescence, these techniques are generally more complex and require more sophisticated instrumentations in term of excitation source, detection and electronics. In particular a pulsed source of excitation is needed, and generally provided by a pulsed laser. In this work, a Ti:sapphire laser is used as excitation source providing short pulses with 1-2 ps FWHM at a repetition rate of 82 MHz and at a wavelength that can be tuned in the range 725-1000 nm. Two methods are used: Time-Correlated-Single-Photon-Counting (TCSPC) and a streak camera system. The principles of both techniques are described in more detail below. Both use the same set up for the excitation source and partly use the same electronics but differ from each other by the mode of detection. In TCSPC, the emitted photons are generally collected by a thermoelectrically cooled micro-channel plate photomultiplier tube, while the streak camera system uses a spectrometer combined with a CCD camera to collect the photons.

Typically in a time-resolved fluorescence experiment, the sample is excited with a short pulse of light and its fluorescence intensity decay is measured as function of time. The fluorescence intensity decay of a fluorophore is typically assumed to decay as the sum of single exponential decays as in Equation 4.3.[36]

$$I(t) = I_0 \sum_{i}^{n} \alpha_i \exp\left(-t/\tau_i\right) \tag{4.3}$$

In this expression, I_0 is the intensity at time zero, τ_i are the fluorescence lifetimes, α_i correspond to the amplitudes of the components at time zero and n is the number of components.

Time-Correlated-Single-Photon-Counting

Time-correlated-single-photon-counting (TCSPC) is one of the most commonly used techniques for measuring time-resolved fluorescence decays. Time-resolution is obtained by recording the temporal difference between the excitation pulse and the detection of a single photon emitted by the sample.[36] When the laser pulse is detected by a photodiode, a Time-to-Amplitude-Converter (TAC) is triggered and starts an increasing with time voltage ramp. As the first photon emitted by the sample hits the detector, the TAC is stopped. The acquired voltage is then converted into a corresponding time via the use of an Analog-to-Digital-Converter (ADC). This time is then stored in one of the channels of a Multi-Channel Analyzer (MCA). By counting many of these events, one can build a histogram of counted photons versus time that represents the fluorescence decay of the sample. A schematic of the experimental set up and the principle of TCSPC are shown in Figure 4.6.

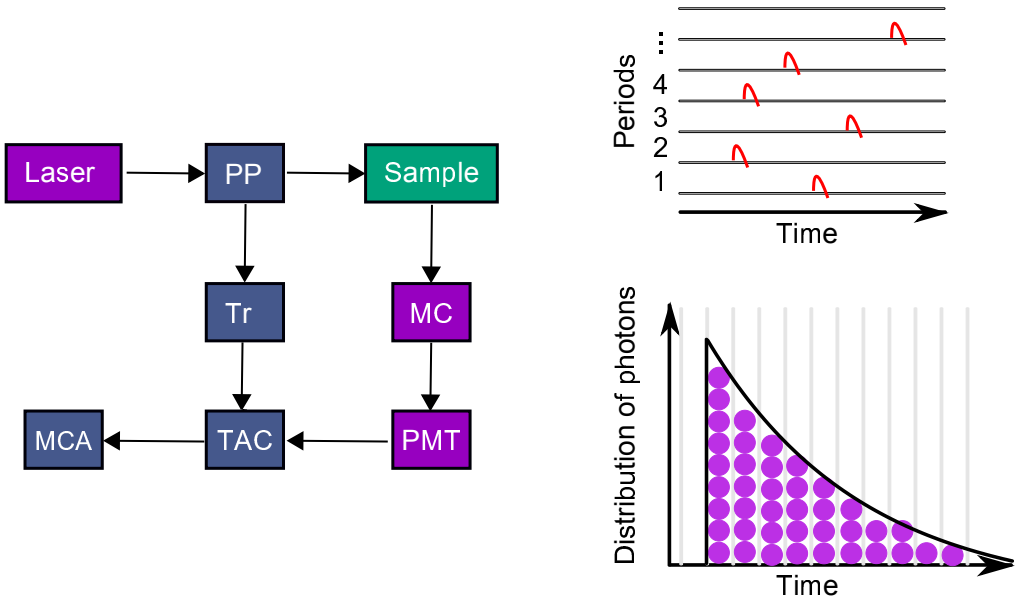

Figure 4.6. (**left**) Schematic of the experimental set up for time correlated single photon counting consisting of a Pulse Picker (PP), a Trigger (Tr), a Time-to-Amplitude Converter (TAC), a Multi-Channel Analyzer (MCA), a Monochromator (MC) and a Photomultiplier Tube (PMT); (**right**) Schematic representation showing how the photons are randomly detected after a certain time delay and how the counted photons are stored in the MCA to obtain a histogram representation of the intensity decay.

However the measured fluorescence decay is a convolution of the real fluorescence intensity decay and the Instrument Response Function (IRF) which represents how the excitation pulse appears to the detector. Thus a TCSPC measurement requires to record two set of data: one is the fluorescence decay of the sample and the other one is the IRF which is

measured by directing the laser pulse to the detector using a scattering solution. For good statistics, both the fluorescence decays and the IRF are measured with 10 000 photons in their top channel. The shape of the IRF depends on the type of detector and the width of the excitation pulse and the former is typically larger due to the transit time spread of the photoelectrons in the detector. The real decay of the sample can be obtained by deconvolution of the measured data with the IRF. To avoid any polarization effects on the lifetime measurements, a polarizer in the detection system set at 54.7º (magic angle) to the polarization plane of the excitation light is used. In the TCSPC measurements presented in Paper II, a NIR detector (R3809U-50, Hamamatsu) was used with an IRF width of ca. 110 ps.

In TCSPC, it is also important to adjust the measurement conditions so that only 1 photon is detected per laser pulse, since the electronics are not fast enough to detect all photons simultaneously as it needs to reset after each photon detected. Moreover at high emission intensity, there is a non-negligible probability for two photons originating from the same excitation event to hit the detector. Due to the dead-time of the detector after detection, the first photon will be counted but the second one will not be counted, resulting in a fluorescence decay biased toward early photons and a shorter lifetime than expected. To avoid this "pile-up" effect, the emission intensity is reduced so that only 1 photon is detected per every 100 excitation pulses.

Streak camera

A streak camera system can also be used to record fluorescence decay over time. As mentioned previously, this technique differs from TCSPC by the mode of detection and presents two strong advantages. First a better time resolution can be obtained with a time resolution of ca. 15 ps in the time scale used for streak camera measurements presented in Paper II. The second advantage is that it makes possible the measurement of the fluorescence intensity versus both time and wavelength within a single experiment. By combining a spectrometer and a CCD-camera, a streak camera system allows the measurement of time variation of the incident light intensity with respect to the wavelength. A schematic representation of the streak camera system used is shown in Figure 4.7.

The emitted photons are first dispersed by wavelength on a line using the spectrometer and then arrive on a photocathode. On the photocathode, the emitted photons (or optical pulses) are converted sequentially into a number of electrons according to their intensity. These electrons are then accelerated and pass through a pair of sweep electrodes on which a high voltage is applied. As they pass through this high voltage sweep, the electrons are deflected at different angles in the vertical direction, depending on their arrival time. Finally the electrons are multiplied in a micro-channel photomultiplier (MCP) before hitting a phosphor screen where they are again converted into light.

On the phosphor screen, the phosphor image corresponding to the earliest photon is placed on top while the other photons are arranged in sequential order from top to bottom. The intensity of the incident light is given by the brightness of the superimposed phosphor images.

Thus 3D-images of the fluorescence emission can be produced with time along the vertical axis, the wavelength along the horizontal axis and the intensity along the z-axis.

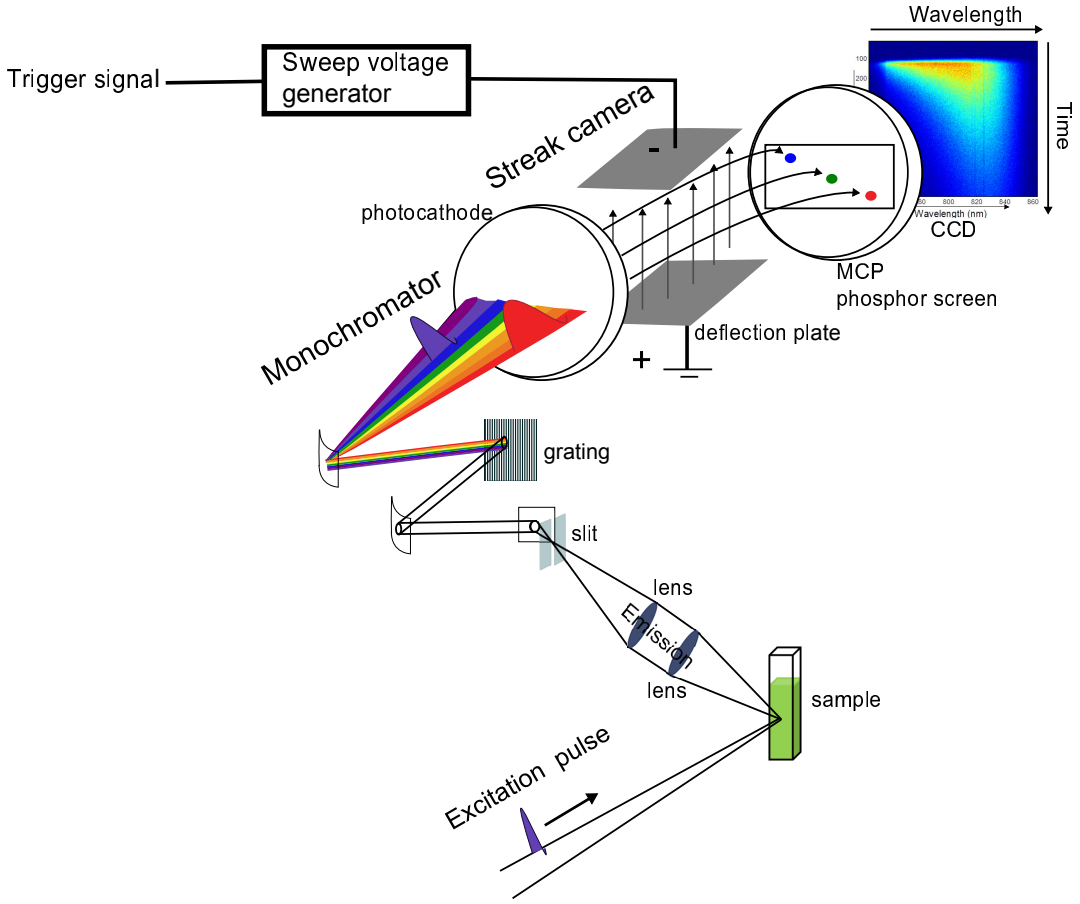

Figure 4.7. Schematic representation of the streak camera system used.[78]

Influence of Conformational Dynamics on Electron Transfer in Porphyrin Oligomer-Fullerene Systems

This second paper investigates how conformation influences the charge-separation processes in long butadyine-linked porphyrin oligomer-fullerene systems $\mathbf{P_n}C_{60}$ (n = 4, 6). In the ground state, the low barrier for rotation of individual porphyrin sub-units results in a wide distribution of conformers. Previous studies on the dimer $\mathbf{P_2}$ have shown that the conformational state of the oligomer (twisted/planar) could be controlled by varying the excitation wavelength.[55] In particular, in the Q band, twisted conformers were found to absorb at short wavelengths, while more planar conformations absorbed at longer wavelengths. The conformational distribution could also be restrained and controlled by coordination to multidentate ligand. Thus in the presented work, two approaches are explored to study the conformational dependence of charge separation in long oligomers $\mathbf{P_n}C_{60}$ (n = 4, 6).

In the first approach, tuning the excitation wavelength makes it possible to prepare different initial excited states in term of conformations (twisted/planar). Figure 4.8 shows the absorption spectra of $\mathbf{P_4}C_{60}$ and $\mathbf{P_6}C_{60}$ together with the absorption spectra of the donor systems $\mathbf{P_n}$ (n = 4, 6) as reference. The arrows indicate the excitation wavelengths chosen to selectively excite different populations of conformers. For both systems, short excitation wavelengths (λ < 800 nm) bring predominantly twisted conformations in the excited state, while at longer excitation wavelengths (λ > 800 nm), more planar conformations are excited. In the second approach, charge separation is explored in constrained systems. Semi-circular complexes $\mathbf{P_n}C_{60}$-$\mathbf{T_8}$ were obtained by coordination of $\mathbf{P_n}C_{60}$ to an octadentate ligand $\mathbf{T_8}$, that hinders the rotation of individual porphyrin units. Figure 4.8 provides the absorption spectra of the semi-circular complexes $\mathbf{P_4}C_{60}$-$\mathbf{T_8}$ and $\mathbf{P_6}C_{60}$-$\mathbf{T_8}$ along with the spectra of the respective reference systems $\mathbf{P_n}$-$\mathbf{T_8}$. As shown in Figure 4.9, coordination of the Zn centers to the pyridine groups of the template $\mathbf{T_8}$ forces the oligomer to adapt a more planar conformation. This leads to dramatic spectral changes, mostly in the Q band, with the presence of a new red-shifted peak and a more structured Q band due to the more narrow conformational distribution (Figure 4.9).

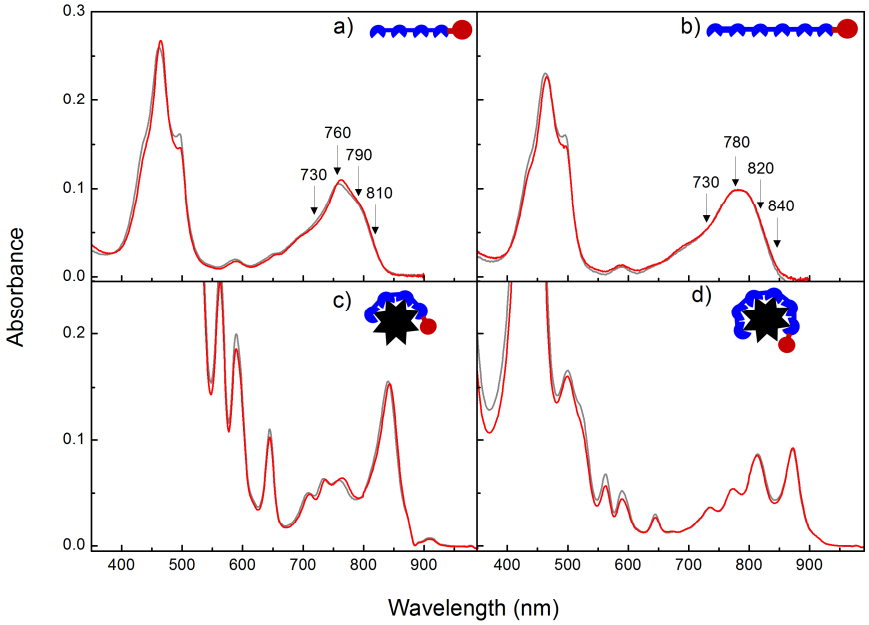

Figure 4.8. (**top**) Ground-state absorption spectra of the linear systems: (**a**) $\mathbf{P_4}C_{60}$ (red) and (**b**) $\mathbf{P_6}C_{60}$ (red) in 2-MTHF with 1% pyridine added. (**bottom**) Ground-state absorption spectra of the semi-circular complexes: (**c**) $\mathbf{P_4}C_{60}$-$\mathbf{T_8}$ (red) and (**d**) $\mathbf{P_6}C_{60}$-$\mathbf{T_8}$ (red) in DCM/Toluene (60/40) with 0.1% pyridine added. The absorption spectra of the reference systems $\mathbf{P_n}$ and $\mathbf{P_n}$-$\mathbf{T_8}$ systems are plotted in gray. All measurements were done at room temperature.

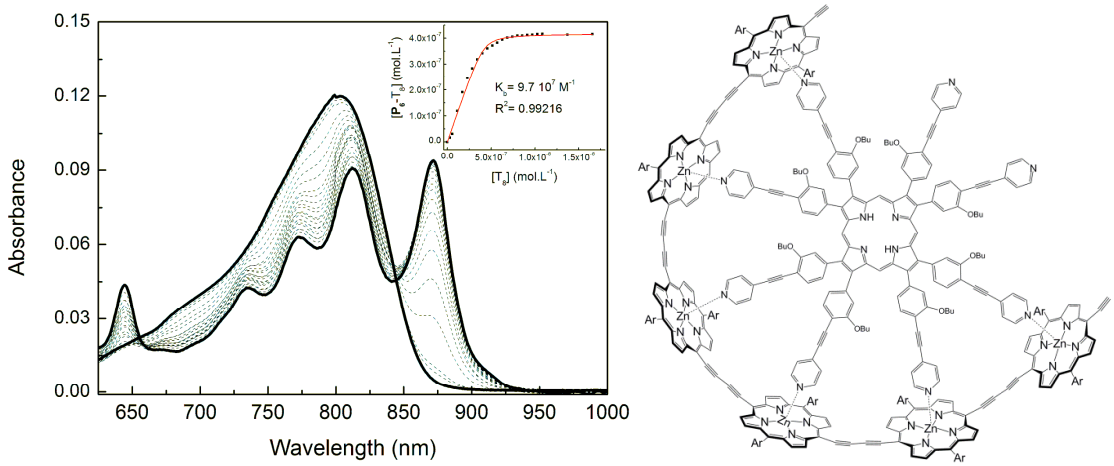

Figure 4.9. (**left**) The Q band region of $\mathbf{P_6}$. A solution of $\mathbf{P_6}$ titrated by the octadentate ligand $\mathbf{T_8}$ in DCM/Toluene (60/40) with 0.1% pyridine added. The total concentration of $\mathbf{P_6}$ was approximately 0.4 μM. Inset concentration of $\mathbf{P_6}$-$\mathbf{T_8}$ complex formed vs. concentration of template $\mathbf{T_8}$ added with fitted binding curve yielding K_b= 9.7 x 10^7 M^{-1}. (**right**) Molecular structure of the semi-circular complex $\mathbf{P_6}$-$\mathbf{T_8}$.

To obtain a more complete understanding of the influence of conformation on the charge separation requires varying the excitation energy while monitoring the emission. Both steady-

state and 2D time-resolved fluorescence emissions were used to obtain information on the charge-separation process in un-constrained $\mathbf{P_n}C_{60}$ and constrained $\mathbf{P_n}C_{60}$-$\mathbf{T_8}$. Figure 4.10 compares the quantum yield for charge separation for both the linear systems and the semi-circular complexes as function of the excitation wavelength, determined by steady-state and time-resolved methods.

Steady-state measurements show moderately small variations of the quantum yield with the excitation wavelength for the $\mathbf{P_n}C_{60}$ compounds. Nevertheless a larger quantum yield for charge separation was observed when exciting predominantly twisted conformers (λ_{exc} = 730 nm and λ_{exc} = 780 nm for $\mathbf{P_6}C_{60}$). Smaller variations of the quantum yield for charge separation were observed for $\mathbf{P_4}C_{60}$ when varying the excitation wavelength that could be explained by the more narrow distribution of conformers of $\mathbf{P_4}C_{60}$ compared to $\mathbf{P_6}C_{60}$. The semi-circular complexes showed wavelength independent and much lower quantum yield for charge separation than their linear counterparts. This absence of dependency on the excitation wavelength could be explained by the increased rigidity and planarity of these semi-circular complexes.

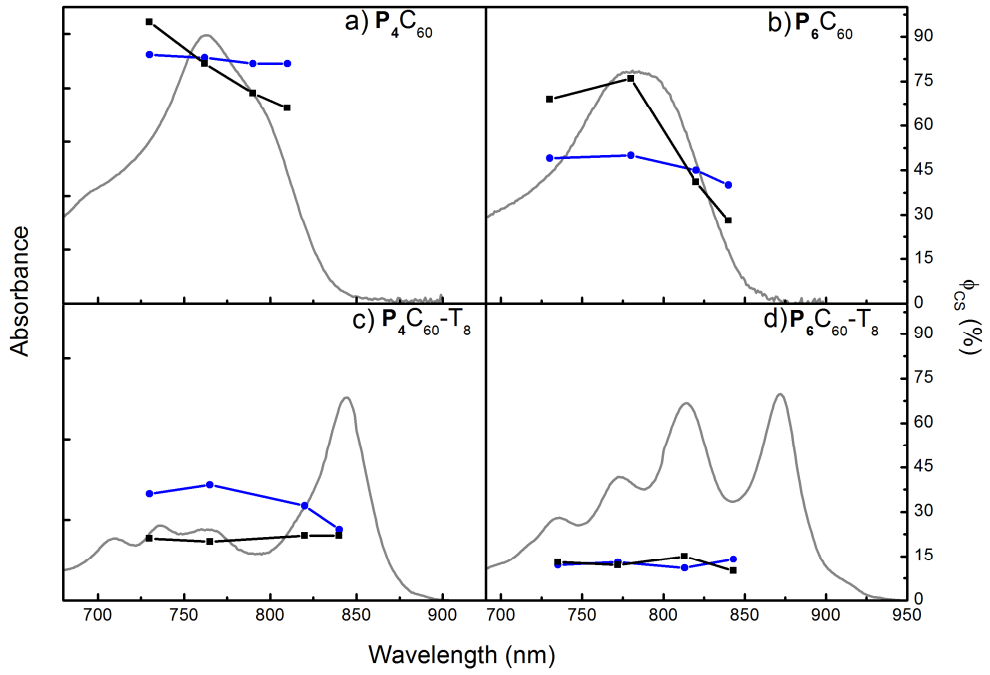

Figure 4.10. (**top**) Quantum yield for charge separation as function of the excitation wavelength based on steady-state (blue) and time-resolved fluorescence (black) measurements for (**a**) $\mathbf{P_4}C_{60}$ and (**b**) $\mathbf{P_6}C_{60}$ in 2-MTHF with 1% pyridine added at 300 K. (**bottom**) Quantum yield for charge separation as function of the excitation wavelength based on steady-state (blue) and time-resolved fluorescence (black) measurements for (**c**) $\mathbf{P_4}C_{60}$-$\mathbf{T_8}$ and (**d**) $\mathbf{P_6}C_{60}$-$\mathbf{T_8}$ in DCM/Toluene (60/40) with 0.1 % pyridine added at 300 K. The values obtained from steady-state measurements were calculated as $1\text{-}I_f(\mathbf{P_n}C_{60})/I_f(\mathbf{P_n})$, where the I_f's are the integrated fluorescence intensities from samples of $\mathbf{P_n}C_{60}$ and $\mathbf{P_n}$ with equal absorbance at the excitation wavelength. The respective Q band regions of the absorption spectra are shown in grey.

Stronger evidence of the conformational dependence of the charge separation comes from 2D time-resolved measurements. 2D streak camera images of both the reference systems $\mathbf{P_n}$ and the donor-acceptor systems $\mathbf{P_n}C_{60}$ were recorded with the same excitation wavelengths used in steady-state. As an example, Figure 4.11 provides the 2D streak camera images of the emission of $\mathbf{P_6}C_{60}$ at 300 K excited at 730 nm, 780 nm, 820 nm and 840 nm. For all systems $\mathbf{P_n}$ and $\mathbf{P_n}C_{60}$, multi-exponential fluorescence decays are observed that depend on both excitation and emission wavelengths. In general, fast fluorescence decays dominate the emission when exciting twisted conformations (λ_{exc} < 800 nm) while excitation of planar conformations (λ_{exc} > 800 nm) results in slower fluorescence decays. Unlike the linear systems, the semi-circular complexes show a much simpler behavior with mono-exponential fluorescence decays independent on both excitation and emission wavelengths. Table 4.3 provides the fitted lifetimes of $\mathbf{P_n}C_{60}$-$\mathbf{T_8}$ complexes as function of the excitation wavelength, along with the fitted lifetimes of their respective reference systems $\mathbf{P_n}$-$\mathbf{T_8}$. The fullerene-appended systems present slightly shorter lifetimes than the reference systems that results in a slow rate constant and low efficiency of charge separation in agreement with steady-state measurements.

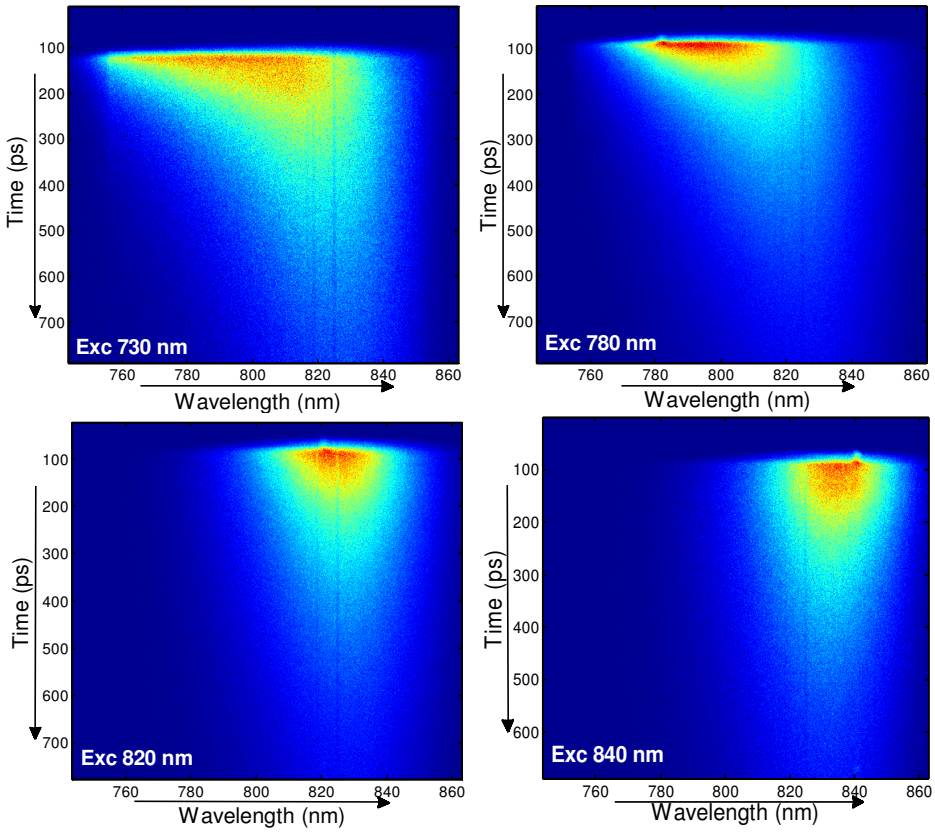

Figure 4.11. 2D streak camera images of the emission of $\mathbf{P_6}C_{60}$ at 300 K in 2-MTHF with 1% pyridine excited at 730 nm (top left), 780 nm (top right), 820 nm (bottom left) and 840 nm (bottom right). The small shoulder observed at ca. 780 nm, 820 nm and 840 nm on the 2D images is due to a small amount of directly scattered excitation light that could not be avoided during the measurements, but this did not significantly affect the fitting procedure.

Table 4.3. Fluorescence lifetimes τ_f, rate constants for charge separation k_{CS} and quantum yield for charge separation ϕ_{CS} for P_nC_{60}-T_8 complexes

Tetramer System				
λ_{exc} / nm	τ_f (**P_4-T_8**) [a] / ps	τ_f (**P_4C_{60}-T_8**) [a] / ps	k_{CS} [c] / s^{-1}	ϕ_{CS} [d]
735	499	398	5.1 x 10^8	0.20
765	499	405	4.7 x 10^8	0.19
820	527	414	5.2 x 10^8	0.21
840	530	417	5.1 x 10^8	0.21
Hexamer System				
λ_{exc} / nm	τ_f (**P_6-T_8**)[b] / ps	τ_f (**P_6C_{60}-T_8**)[b] / ps	k_{CS} [c] / s^{-1}	ϕ_{CS} [d]
735	430	374	3.5 x 10^8	0.13
772	432	382	3.0 x 10^8	0.12
813	448	382	3.9 x 10^8	0.15
843	443	397	2.6 x 10^8	0.10

[a] The lifetimes were obtained from the fitting of the fluorescence decays measured using TCSPC. [b] The lifetimes were obtained from the fitting of the fluorescence decays measured using a streak camera system. [c] The charge separation rate constant k_{CS} was determined using the formula $k_{CS} = 1/\tau_f$ (**P_nC_{60}-T_8**) – $1/\tau_f$ (**P_n-T_8**). [d] The quantum yield for charge separation ϕ_{CS} was calculated as $\phi_{CS} = k_{CS} \cdot \tau_f$ (**P_nC_{60}-T_8**).

To benefit from the increased information content of the 2D streak camera images, a singular-value-decomposition (SVD) method combined with a decay model based on structural relaxation of the twisted conformers into more planar conformers was developed. Indeed previous studies have shown that in the excited state, twisted conformations are less stable and tend to relax to more planar conformations before emission.[55] Figure 4.12 shows the three-state model used to describe the relaxation (via planarization) of the porphyrin oligomers with $\mathbf{P_n}^{\#}$, $\mathbf{P_n}^{¤}$ and $\mathbf{P_n}^{*}$ corresponding to a twisted, intermediately twisted and planarized oligomer in the excited state, respectively. In the $\mathbf{P_nC_{60}}$ systems, charge separation could occur from either non-relaxed or relaxed states. All the rate constants related to planarization ($\mathbf{k_1}$, $\mathbf{k_2}$) and natural decays ($\mathbf{k}^{\#}$, $\mathbf{k}^{¤}$, $\mathbf{k}^{*}$) were fixed to the values obtained from the fitting decays of the reference systems $\mathbf{P_n}$. From this SVD-based analysis, both kinetics and spectral changes taking place in the excited state could be analyzed for the different

conformers. As an example, the results of this analysis for a sample of $\mathbf{P_6}C_{60}$ excited at 730 nm are shown in Figure 4.13. Three conformational populations contribute to the emission. The first one emits mostly at short wavelength and corresponds to mostly twisted conformations while the third one populated by two consecutive relaxations emits at the red end of the spectrum and represents more planar conformations. This gradual red-shift in wavelength emission with increasing time was observed for all systems studied showing that relaxation competes effectively with the charge separation process in the excited state. Comparison of the measured (Figure 4.13 a) and the reconstructed (Figure 4.13 b) 2D images shows a reasonably good fit and supports the validity of the proposed model. The rate constants for the charge separation were also derived from SVD analysis for both $\mathbf{P_4}C_{60}$ and $\mathbf{P_6}C_{60}$ compounds (Table 4.4). Charge separation occurs mostly from non-relaxed states with larger rate constants observed when exciting twisted conformations (λ_{exc} = 730 nm for both $\mathbf{P_4}C_{60}$ and $\mathbf{P_6}C_{60}$). As an example for the $\mathbf{P_6}C_{60}$ compound, excitation of twisted conformers results in a charge separation rate constant $\mathbf{k}_{CS}^{\#}$ at least 20 times larger for non-relaxed states than for the more planar relaxed states ($\mathbf{k}_{CS}^{¤}$ and $\mathbf{k}_{CS}^{*}$).

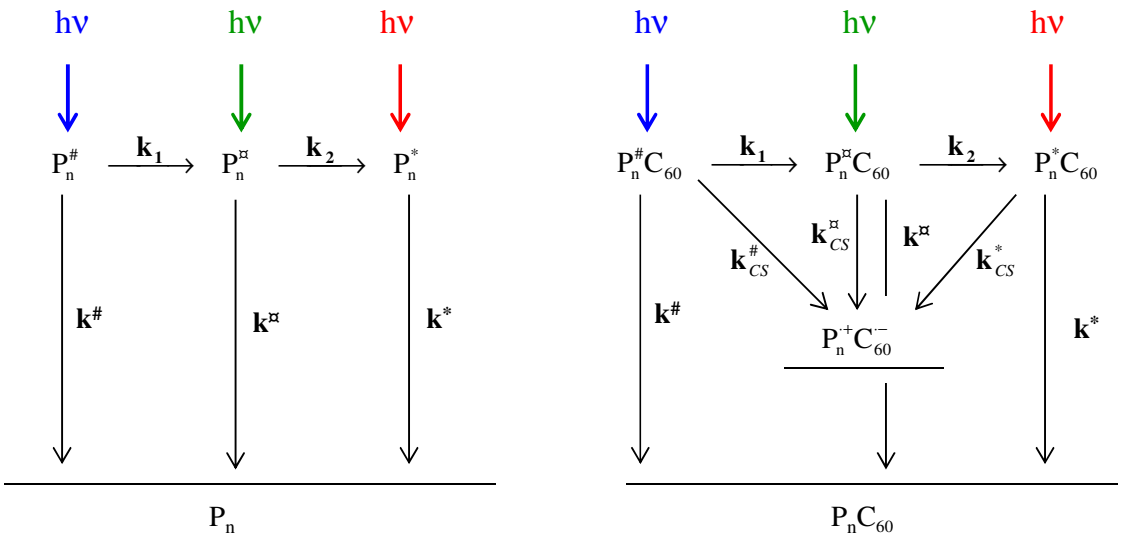

Figure 4.12. Kinetic model used to describe structural relaxation and charge separation in the studied systems. (**Left**) Model $\mathbf{P_n}$ systems; (**Right**) Donor-acceptor $\mathbf{P_n}C_{60}$ systems. The different rate constants involved are explained in the text.

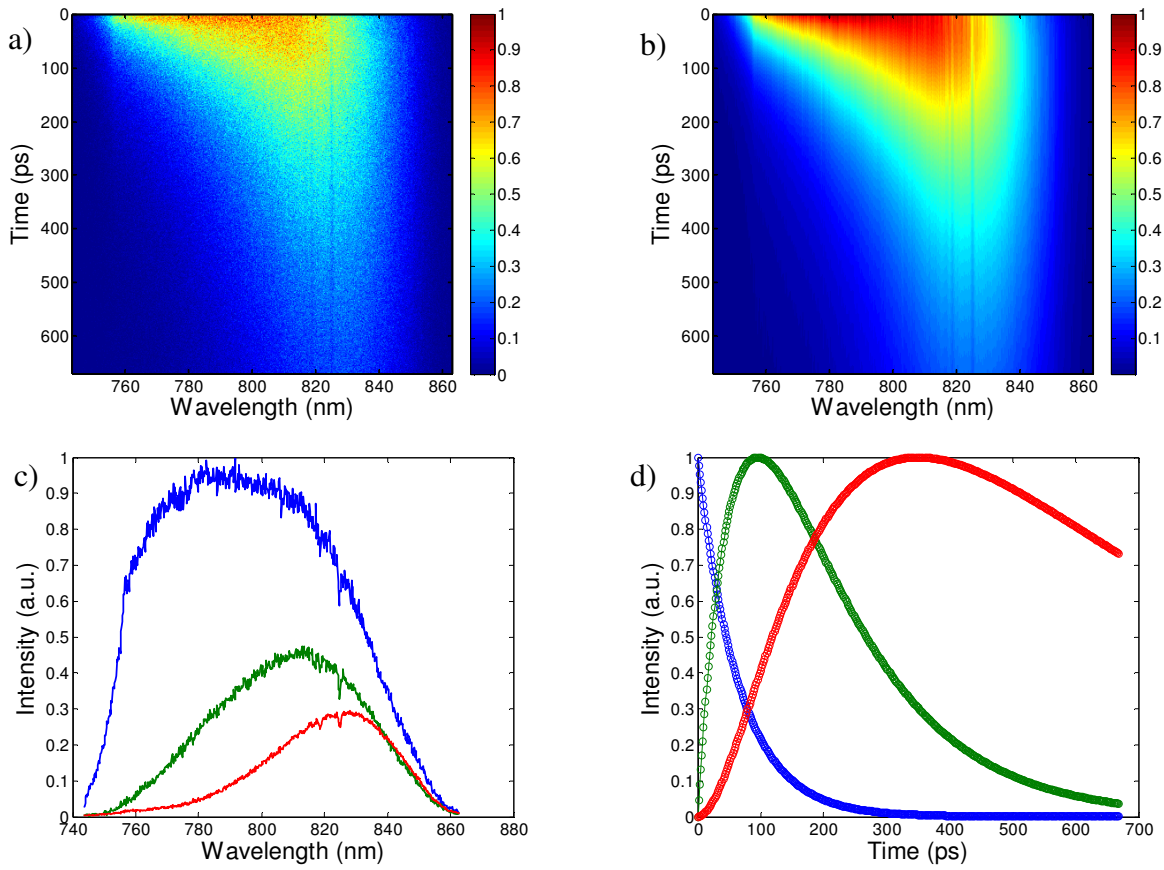

Figure 4.13. a) Normalized 2D streak camera image of the emission of $\mathbf{P_6C_{60}}$ excited at 730 nm at 300 K in 2-MTHF with 1% pyridine. b) Reconstructed 2D image of the emission of $\mathbf{P_6C_{60}}$ excited at 730 nm. This image was built from the data obtained in the fitting procedure. c) Spectral components and d) fluorescence decays of the 3 species contributing to the fluorescence emission. The color code used in c) and d) is the same, i.e. the fluorescence decay in blue corresponds to the species with the blue emission etc.

Table 4.4. Wavelength Dependence of the charge separation rate constants for $\mathbf{P_6C_{60}}$ and $\mathbf{P_4C_{60}}$ at 300 K

$\mathbf{P_4C_{60}}$				$\mathbf{P_6C_{60}}$			
λ_{exc}/ nm	$k_{cs}^{\#}/10^9\ s^{-1}$	$k_{cs}^{¤}/10^9\ s^{-1}$	$k_{cs}^{*}/10^9\ s^{-1}$	λ_{exc}/ nm	$k_{cs}^{\#}/10^9\ s^{-1}$	$k_{cs}^{¤}/10^9\ s^{-1}$	$k_{cs}^{*}/10^9\ s^{-1}$
730	13.1	2.7	0.9	730	8.6	0.0	0.3
760	14.9	2.7	0.0	780	8.8	2.8	0.5
790	-	7.4	1.5	820	-	3.3	0.5
810	-	6.0	0.6	840	-	0.0	0.9

As described in Chapter 2, the electron transfer rate depends on several parameters: the thermodynamic driving force, the reorganization energy and the electronic coupling. As demonstrated above and in previous studies,[55,57] twisted conformations of $\mathbf{P_n}C_{60}$ lie at higher energy in the excited state, and hence a larger driving force for direct charge separation from these states is expected. Unlike twisted conformers, planar conformers due to the increased conjugation are more stabilized in the excited state. Consequently they lie closer to the charge-separated state energy level that results in a smaller driving force for charge-separation to occur. Thus the observed disparity in charge separation rate constants was partly attributed to the difference in driving force between twisted and planar conformations. In Figure 4.14, the energy diagram illustrates the variation of the driving force for charge separation with respect to the excited state conformation for the entire series $\mathbf{P_n}C_{60}$ (n = 1-4, 6). Finally strong evidence for the driving force as determining factor in the charge separation in long oligomers $\mathbf{P_n}C_{60}$ comes from the time-resolved measurements on the semi-circular complexes $\mathbf{P_n}C_{60}$-$\mathbf{T_8}$. These semi-circular complexes show slow rate constants for charge separation compared to their linear counterparts. Due to their almost planar conformations, the excited state of these complexes is estimated to lie very close to the charge-separated state level and hence a small driving force for charge separation can be expected. Thus these results show how the control of the conformational state of these oligomers can be used to tune the rate of charge separation.

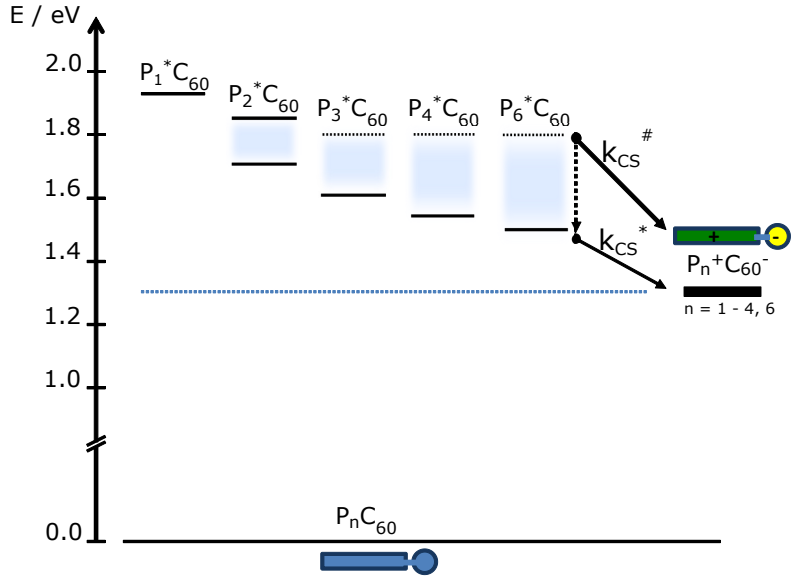

Figure 4.14. Energy diagram for the charge separation process estimated from spectroscopic data. The distribution of conformers gets broader as the length of the oligomer increases.

5. *Summary and Future Perspective*

This thesis has been focused on understanding the effects of conformation on the photophysical properties of porphyrin oligomers $\mathbf{P_n}$ and on the charge separation processes in the porphyrin-based donor acceptor systems $\mathbf{P_n}C_{60}$.

It was first shown that these porphyrin oligomers could self-assemble in well-defined and planar aggregates at low temperatures. The formation of these small aggregates, probably dimers, was characterized by dramatic changes in the spectral properties of the oligomers $\mathbf{P_n}$ that could be attributed to a planarization of the oligomers accompanying the aggregate formation. More interestingly, systems with appended electron donor and/or acceptor, $\mathbf{P_n}C_{60}$ and Fc$\mathbf{P_n}C_{60}$ could also formed similar small stacked aggregates at low temperatures, providing thus new model systems for investigating charge migration. In particular these aggregates could be used to investigate the effect of planarization on the charge separation and recombination processes in Fc$\mathbf{P_n}C_{60}$ systems.

The effect of conformation on the charge separation process was studied thoroughly in long donor-acceptor systems $\mathbf{P_n}C_{60}$ (n = 4, 6). Compared to shorter oligomers,[57] long oligomers show a more complex behavior in the excited state with a competition between relaxation (via planarization) and charge separation processes. The charge separation rate could be tuned by selective excitation of different populations of conformers. For both systems studied, twisted conformations show a faster charge separation rate constant than planar conformations. This difference in charge separation rates was attributed to a difference in driving force with respect to the excited conformations. In the excited state, twisted conformations lying higher in energy than planar conformations benefit from a larger driving force for charge separation to occur and hence show faster charge separation rate constants. To obtain a simpler model system for charge separation, the conformational distribution could also be controlled and restrained using an octadentate ligand $\mathbf{T_8}$ that forced both oligomers $\mathbf{P_n}C_{60}$ (n = 4, 6) to adopt a semi-circular conformation. These semi-circular complexes $\mathbf{P_n}C_{60}$-$\mathbf{T_8}$ show a slow rate constant and a low efficiency of charge separation that was explained by the small driving force resulting from the increased planarity of these systems. In future it could be interesting to extend this study by probing the excitation wavelength dependence of the charge separation and recombination processes of Fc$\mathbf{P_n}C_{60}$ systems.

6. Acknowledgements

I would like to express my sincere gratitude to the following persons:

My supervisor Bo Albinsson for having accepted me in the Balb group, for introducing me to the field of laser and electron transfer, and finally for your support and guidance.

My co-supervisor Maria Abrahamsson for your encouragement, valuable advice and interesting scientific discussions.

Joakim and Jonas for everything you taught me on lasers and your patience in the laserlab.

Joachim, Damir, Maria for the great discussions in our article-meeting. I miss it !

Anke, Tamas, Lulu for bringing a friendly and inspiring atmosphere in our office.

All people at floor 5 for the great atmosphere.

Enfin un grand merci à mes parents et mes frères pour votre encouragement et continuel soutien malgré les distances.

Et un grand merci également à Hithesh: sans toi rien de ceci n'aurait été possible.

7. References

(1) *30 Key Energy Trends in the IEA and World Wide*; International Energy Agency, 2005.

(2) Morton, O. *Nature* **2006**, *443*, 19.

(3) Gust, D.; Moore, T. A. *Science (New York, N.Y.)* **1989**, *244*, 35.

(4) Bard, A. J.; Fox, M. A. *Accounts of Chemical Research* **1995**, *28*, 141.

(5) Magnuson, A.; Frapart, Y.; Abrahamsson, M.; Horner, O.; Åkermark, B.; Sun, L.; Girerd, J.-J.; Hammarström, L.; Styring, S. *Journal of the American Chemical Society* **1998**, *121*, 89.

(6) Wasielewski, M. R. *The Journal of Organic Chemistry* **2006**, *71*, 5051.

(7) Wasielewski, M. R., O'Neil, M.P. , Gosztola, D. , Niemczyk, M.P. and Svec, W.A. *Pure & Appl. Chem.* **1992**, *64*, 1319.

(8) Steinberg-Yfrach, G.; Rigaud, J.-L.; Durantini, E. N.; Moore, A. L.; Gust, D.; Moore, T. A. *Nature* **1998**, *392*, 479.

(9) Kodis, G.; Terazono, Y.; Liddell, P. A.; Andréasson, J.; Garg, V.; Hambourger, M.; Moore, T. A.; Moore, A. L.; Gust, D. *Journal of the American Chemical Society* **2006**, *128*, 1818.

(10) Balzani, V.; Credi, A.; Venturi, M. *ChemSusChem* **2008**, *1*, 26.

(11) Magnuson, A.; Berglund, H.; Korall, P.; Hammarstrom, L.; Akermark, B.; Styring, S.; Sun, L. C. *Journal of the American Chemical Society* **1997**, *119*, 10720.

(12) Hammarstrom, L.; Hammes-Schiffer, S. *Accounts of Chemical Research* **2009**, *42*, 1859.

(13) Gust, D.; Moore, T. A.; Moore, A. L.; Lee, S.-J.; Bittersmann, E.; Luttrull, D. K.; Rehms, A. A.; DeGraziano, J. M.; Ma, X. C.; Gao, F.; Belford, R. E.; Trier, T. T. *Science* **1990**, *248*, 199.

(14) Kadish, K. M.; Smith, K. M.; Guilard, R. *The porphyrin handbook: Electron transfer*; Academic Press, 2003.

(15) Nishitani, S.; Kurata, N.; Sakata, Y.; Misumi, S.; Karen, A.; Okada, T.; Mataga, N. *Journal of the American Chemical Society* **1983**, *105*, 7771.

(16) Gust, D.; Moore, T. A.; Moore, A. L. *Accounts of Chemical Research* **2000**, *34*, 40.

(17) Gust, D.; Moore, T. A. In *Advances in Photochemistry*; John Wiley & Sons, Inc.: 2007, p 1.

(18) Gust, D.; Moore, T. A.; Moore, A. L. *Accounts of Chemical Research* **1993**, *26*, 198.

(19) Gust, D.; Moore, T. A.; Moore, A. L. *Accounts of Chemical Research* **2009**, *42*, 1890.

(20) Guldi, D. M. *Chemical Society Reviews* **2002**, *31*, 22.

(21) Imahori, H.; Sakata, Y. *European Journal of Organic Chemistry* **1999**, *1999*, 2445.

(22) Wasielewski, M. R. *Chemical Reviews* **1992**, *92*, 435.

(23) Borgstrom, M.; Shaikh, N.; Johansson, O.; Anderlund, M. F.; Styring, S.; Akermark, B.; Magnuson, A.; Hammarstrom, L. *Journal of the American Chemical Society* **2005**, *127*, 17504.

(24) Aviram, A.; Ratner, M. A. *Chemical Physics Letters* **1974**, *29*, 277.

(25) Balzani, V.; Credi, A.; Venturi, M. *ChemPhysChem* **2003**, *4*, 49.

(26) Balzani, V. *Photochemical & Photobiological Sciences* **2003**, *2*, 459.

(27) Ball, P. *Nature* **2000**, *406*, 118.

(28) Joachim, C.; Gimzewski, J. K.; Aviram, A. *Nature* **2000**, *408*, 541.

(29) Lin, V.; DiMagno, S.; Therien, M. *Science* **1994**, *264*, 1105.

(30) Anderson, H. L. *Chem. Commun.* **1999**, 2323.

(31) Anderson, H. L.; Martin, S. J.; Bradley, D. D. C. *Angewandte Chemie International Edition in English* **1994**, *33*, 655.

(32) Marcus, R. A. *J. Chem. Phys.* **1956**, *24*, 966.

(33) Hush, N. S. *J. Chem. Phys.* **1958**, *28*, 962.

(34) Levich, V. *Adv. Electrochem. Eng.* **1966**, *4*, 249.

(35) Hollas, J. M. *Modern Spectroscopy. Fourth Edition*; Johns Wiley & Sons: Hoboken, NJ, 2004.

(36) Lakowicz, J. R. *Principles of Fluorescence Spectroscopy. Third Edition*; Springer: New-York, NY, 2006.

(37) Marcus, R. A. *Can. J. Chem.* **1959**, *37*, 155.

(38) Marcus, R. A. *JCP* **1965**, *43*, 679.

(39) Marcus, R. A.; Sutin, N. *Biochim. Biophys. Acta* **1985**, *811*, 265.

(40) Weller, A. *Z. Phys. Chem.* **1982**, *133*, 93.

(41) Amashukeli, X., Gruhn, N. E., Lichtenberger, D. L. et al. *J. Am. Chem. Soc.* **2004**, *126*, 15566.

(42) Hilgendorff, M., Sundström, V. *Chem. Phys. Lett.* **1998**, *287*, 709.

(43) Barber, J. *Chemical Society Reviews* **2009**, *38*, 185.

(44) Blankenship, R. E.; Tiede, D. M.; Barber, J.; Brudvig, G. W.; Fleming, G.; Ghirardi, M.; Gunner, M. R.; Junge, W.; Kramer, D. M.; Melis, A.; Moore, T. A.; Moser, C. C.; Nocera, D. G.; Nozik, A. J.; Ort, D. R.; Parson, W. W.; Prince, R. C.; Sayre, R. T. *Science* **2011**, *332*, 805.

(45) Lehn, J. M. *Supramolecular Chemistry: Concepts and Perspectives*; Wiley, 1995.

(46) A. Osuka, N. M. a. T. O. *Pure & Appl. Chem.* **1997**, *69*, 797.

(47) Sheats, J. R. *Journal of Materials Research* **2004**, *19*, 1974.

(48) Moore, T. A.; Gust, D.; Mathis, P.; Mialocq, J.-C.; Chachaty, C.; Bensasson, R. V.; Land, E. J.; Doizi, D.; Liddell, P. A.; Lehman, W. R.; Nemeth, G. A.; Moore, A. L. *Nature* **1984**, *307*, 630.

(49) Gouterman, M. *Optical Spectra and Electronic Structure of Porphyrins and Related Rings*; Academic Press; Vol. 3.

(50) Crossley, M. J.; Burn, P. L. *Journal of the Chemical Society, Chemical Communications* **1987**, *0*, 39.

(51) L. Anderson, H. *Chemical Communications* **1999**, 2323.

(52) Lin, V. S. Y.; Therien, M. J. *Chemistry – A European Journal* **1995**, *1*, 645.

(53) Tsuda, A.; Osuka, A. *Science* **2001**, *293*, 79.

(54) Kim, D.; Osuka, A. *Accounts of Chemical Research* **2004**, *37*, 735.

(55) Winters, M. U.; Kärnbratt, J.; Eng, M.; Wilson, C. J.; Anderson, H. L.; Albinsson, B. *The Journal of Physical Chemistry C* **2007**, *111*, 7192.

(56) Liddell, P. A.; Sumida, J. P.; Macpherson, A. N.; Noss, L.; Seely, G. R.; Clark, K. N.; Moore, A. L.; Moore, T. A.; Gust, D. *Photochemistry and Photobiology* **1994**, *60*, 537.

(57) Winters, M. U.; Kärnbratt, J.; Blades, H. E.; Wilson, C. J.; Frampton, M. J.; Anderson, H. L.; Albinsson, B. *Chemistry – A European Journal* **2007**, *13*, 7385.

(58) Kahnt, A.; Kärnbratt, J.; Esdaile, L. J.; Hutin, M.; Sawada, K.; Anderson, H. L.; Albinsson, B. *Journal of the American Chemical Society* **2011**, *133*, 9863.

(59) Kubista, M.; Sjoback, R.; Eriksson, S.; Albinsson, B. *Analyst* **1994**, *119*, 417.

(60) Kasha, M. *Discussions of the Faraday Society* **1950**, *9*, 14.

(61) Scheibe, G. *Angew. Chem.* **1937**, *50*, 51.

(62) Scheibe, G., Kandler, L. , Ecker, H. *Naturwissenschaften* **1937**, *25*, 75.

(63) Scheibe, G. *Angew. Chem.* **1937**, *50*, 212.

(64) Scheibe, G. *Angew. Chem.* **1936**, *49*, 563.

(65) Jelley, E. E. *Nature* **1936**, *138*, 1009.

(66) Jelley, E. E. *Nature* **1937**, *139*, 631.

(67) Harrison, W. J.; Mateer, D. L.; Tiddy, G. J. T. *The Journal of Physical Chemistry* **1996**, *100*, 2310.

(68) Kirstein, S.; Daehne, S. *International Journal of Photoenergy* **2006**, *2006*.

(69) Ribo, J. M.; Crusats, J.; Farrera, J.-A.; Valero, M. L. *Journal of the Chemical Society, Chemical Communications* **1994**, *0*, 681.

(70) Isago, H. *Chemical Communications* **2003**, *0*, 1864.

(71) Kameyama, K.; Morisue, M.; Satake, A.; Kobuke, Y. *Angewandte Chemie* **2005**, *117*, 4841.

(72) Kameyama, K.; Morisue, M.; Satake, A.; Kobuke, Y. *Angewandte Chemie International Edition* **2005**, *44*, 4763.

(73) Würthner, F.; Thalacker, C.; Diele, S.; Tschierske, C. *Chemistry – A European Journal* **2001**, *7*, 2245.

(74) Johansson, L. B. Å.; Langhals, H. *Spectrochimica Acta Part A: Molecular Spectroscopy* **1991**, *47*, 857.

(75) Hunter, C. A.; Sanders, J. K. M. *Journal of the American Chemical Society* **1990**, *112*, 5525.

(76) Hunter, C. A.; Meah, M. N.; Sanders, J. K. M. *Journal of the American Chemical Society* **1990**, *112*, 5773.

(77) Hoffmann, M.; Karnbratt, J.; Chang, M. H.; Herz, L. M.; Albinsson, B.; Anderson, H. L. *Angew. Chem. Int. Ed.* **2008**, *47*, 4993.

(78) Komura, M.; Itoh, S. *Photosynth Res* **2009**, *101*, 119.